Design Methodology for Wideband Electrically Small Antennas (ESA) Based on the Theory of Characteristic Modes (CM)

DISSERTATION

Presented in Partial Fulfillment of the Requirements for the Degree Doctor of

Philosophy in the Graduate School of The Ohio State University

By

Khaled A. Obeidat, MSEE, BSEE

Graduate Program in Electrical and Computer Engineering

The Ohio State University

2010

Dissertation Committee:

Professor Roberto G. Rojas, Advisor

Professor Robert J. Garbacz

Professor Fernando L. Teixeira

ABSTRACT

Emerging broadband applications with market pressures for miniaturized communication devices have encouraged the use of electrically small antennas (ESA) and highly integrated RF circuitry for high volume low cost mobile devices. This research work focuses on developing a novel scheme to design wideband electrical small antennas that incorporates active and passive loading as well as passive matching networks. Several antennas designed using the proposed design technique and built and measured to assess their performance and to validate the design methodology.

Previously, the theory of Characteristic Modes (CM) has been used mostly for antennas analysis. However; in this chapter a design procedure is proposed for designing wide band (both the input impedance bandwidth and the far field pattern bandwidth) electrically small to mid size antennas using the CM in conjunction with the theory of matching networks developed by Carlin [7].

In order to increase the antenna gain, the antenna input impedance mismatch loss needs to be minimized by carefully exciting the antenna either at one port or at multiple ports and/or load the antenna at different ports along the antenna body such that the Q factor in the desired frequency range is suitable for wideband matching network design. The excitation (feeding structure), the loading of the antenna and/or even small modifications to the antenna structure can be modeled and understood by studying the eigenvalues and their corresponding eigencurrents obtained from the CM of the antenna

structure.

A brief discussion of the theory of Characteristic Modes (CM) will be presented and reviewed before the proposed design scheme is introduced. The design method will be used to demonstrate CM applications to widen the frequency bandwidth of the input impedance of an electrically small Vee shape Antenna and to obtain vertically polarized Omni-directional patterns for such antenna over a wide bandwidth. A loading technique based on the CM to either design frequency reconfigurable antennas or broaden their bandwidth by Non-Foster loading will also be discussed as part of the design methodology.

In the Appendix, a brief discussion of the fundamental limits of electrical small antennas is presented and then followed by a discussion of the fundamental limits of the impedance bandwidth of the ESA when a passive matching network is used. Matching network implemented using Non-Foster matching is also discussed in the appendix.

DEDICATION

To my parents Ahmad and Haya, my wife Manar, my daughter Mona, my sisters Rasha and Luda and my brother Omar

ACKNOWLEDGMENTS

I would like to take this opportunity to express my gratitude to my excellent advisor Prof. Roberto G. Rojas for his guidance and continuous encouragement during my Ph. D. research work. He taught me how to do research systematically and with enthusiasm. I would also like to take this opportunity to thank Prof. Robert J. Garbacz and Prof. Fernando L. Teixeira for their interest and time in agreeing to be part of my dissertation committee.

I would also like to thank all my friends here at ElectroScience Laboratory (ESL), for their support during my PhD study. Special thanks to my research group members for their support and help whenever I needed. I have learned from and had fun with all of my friends here, which made my stay at OSU very enjoyable.

My special thanks to my former advisors during my master degree and my Bachelor degree, namely Prof. Tom Weller and Prof. Nihad Dib. Without their help and support I won't be able to reach where I am in now.

My sincerest thanks to my parents and family without their love and encouragement I would never be the person I am today. I would especially like to thank my mother for being by my side during all the stressful and good times in my life, my daughter Mona who is always proud of her father and finally my wife who never fail to believe in me.

VITA

1999…….. B. S. in Electrical Engineering, Jordan University of Science and Technology, Irbid, Jordan

2003……...M. S. in Electrical Engineering, University of South Florida, Tampa, Florida

PUBLICATIONS

JOURNALS

1. Kamran Entesari, Khaled Obeidat, Andrew Brown and Gabriel M. Rebeiz "A 25-75 MHz RF MEMS Tunable Filter" IEEE Trans. on Microwave Theory and techniques, Volume 55, Issue 11, Nov. 2007 Page(s):2399 – 2405

2. Khaled Obeidat, Bryan D. Raines, and Roberto G. Rojas "Application of Characteristic Modes and Non-Foster Multiport Loading to the Design of Broadband Antennas" Volume 58, Issue 1, January 2010

PATENT

1. Roberto G. Rojas, Khaled Obeidat and Bryan D. Raines "Large Frequency Bandwidth Electrically Small Antennas Loaded with Non-Foster Reactive Elements" Patent Pending (12/139,424)

CONFERENCE PROCEEDINGS

1. Khaled Obeidat, Bryan D. Raines, and Roberto G. Rojas" Analysis of Antenna Input Impedance Resonances in Terms of Characteristic Modes" 2009 USNC/URSI National Radio Science Meeting, Jun, North Charleston, SC

2. Khaled Obeidat, Bryan D. Raines, and Roberto G. Rojas "Design of Antenna Conformal to V-shaped Tail of UAV Based on the Method of Characteristic Modes" EWCA Berlin, Germany, March 23-27, 2009

3. Khaled Obeidat, Bryan D. Raines, and Roberto G. Rojas "Design and Analysis of a Helical Spherical Antenna Using the Theory of Characteristic Modes" 2008 IEEE AP-S International Symposium, San Diego

4. Bryan D. Raines, Khaled Obeidat and Roberto G. Rojas "Characteristic Mode-Based

Design and Analysis of an Electrically Small Planar Spiral Antenna with Omni-directional Pattern" 2008 IEEE AP-S International Symposium, San Diego

5. Khaled Obeidat, Bryan D. Raines, and Roberto G. Rojas" Design of Omni Directional Electrically Small Vee-shaped Antenna Using Characteristic Modes" 2008 USNC/URSI National Radio Science Meeting, January, Boulder, Colorado

6. Khaled Obeidat, Bryan D. Raines, and Roberto G. Rojas, "Broadband Antenna Pattern Synthesis Using Characteristic Modes" 2008 USNC/URSI National Radio Science Meeting, July, Ottawa, Canada

7. Khaled Obeidat, Bryan D. Raines, and Roberto G. Rojas "Antenna Design and Analysis Using Characteristic Modes" 2007 IEEE AP-S International Symposium, Honolulu

8. Al-Zoubi, K. Obeidat, and N. Dib, "Quasi-Static Analysis of Asymmetrical Cylindrical Coplanar Waveguide" 1999 IEEE AP-S Int. Symposium digest, Orlando, FL, pp. 1824-1827, July 1999

FIELDS OF STUDY

Major Field: Electrical and Computer Engineering

TABLE OF CONTENTS

LIST OF TABLES

LIST OF FIGURES

CHAPTER 1

INTRODUCTION

1.1 Background and Motivation

Electrically small wideband antennas have been the subject of extensive research, especially over the past ten years. The goal has been to obtain an antenna with relatively constant pattern and impedance over some desired broad frequency range. Furthermore, market pressures for miniaturizing communication devices have encouraged the use of electrically small antennas with highly integrated RF circuitry. Electrically small antennas (ESA), however, have been shown to be fundamentally limited in bandwidth by the Chu limit [1]; also Wheeler [2] studied the bandwidth limit of small antennas extensively. ESA with ka less than 0.5 exhibit low radiation resistance, high reactance and high Q factor which is inversely proportional to antenna bandwidth. Here, the k is the free space wave number and a is the radius of an imaginary sphere which circumscribes the whole antenna. The fundamental lower Q factor limit was expressed by Chu according to the following inequality:

$$Q \geq \frac{1}{(ka)^3} \quad \text{for } ka < 1 \tag{1.1}$$

Traditionally, matching networks (MN) have been used at the feed points of such

antennas to improve their impedance bandwidth. However, matching networks do not directly address the problem of the excitation of higher order radiation pattern modes at higher frequencies (once the antenna becomes electrically large). Furthermore, for some cases they suffer from loss and are also restricted (Passive Matching Network) by a fundamental limit on the amount of bandwidth improvement as expressed by Fano [16].

In order to stabilize the pattern and impedance over frequency, specialized antenna design techniques have been used. For example, the theories of frequency-independent antennas [3] and ultra-wideband antennas [4], [5], [6] can yield wideband antennas, but these theories only apply to electrically large antennas. Research into similar theories for electrically smaller antennas is ongoing. This work presents a possible framework onto which antenna characteristics may be stabilized over frequency, even if the antenna is electrically small.

A major goal of this work is to use the theory of characteristic modes together with the theory of matching networks to increase both the input impedance bandwidth and the far field pattern bandwidth. Another important goal of this work is to be able to explain the behavior of the antenna input impedance physically as a function of the antenna's feeds and to find a way to determine if a given antenna input impedance is suitable for wideband matching. Finally, it is necessary to develop a technique that utilizes the theory of CM to excite the desired modes and eliminate the undesired modes in the desired frequency band. By properly choosing the number of ports and their location, voltage magnitude and phase, and the type of loads, the current at the feeding port(s) which is inversely proportional to the input impedance, and consequently, the Q factor can be

controlled to some extent. As is well-known, electrically small antennas suffer from a fundamental bandwidth limitation due to their high Q factor (please refer to appendix). In order to be able to approach that fundamental limit, it is desirable to design an antenna with a monotonically decreasing Q factor over the desired frequency band. A damped oscillating behavior of a Q factor is an indication of high order mode excitation and thus is undesirable.

Reconfigurable, yet electrically small antennas, are considered to be a good solution to overcome the bandwidth limitation of electrically small antennas, since in many applications, the instantaneous bandwidth is not wide and mostly narrowband. A loading technique for designing general frequency or pattern reconfigurable antennas based on the theory of CM will be shown to be very effective in resonating the antenna at the desired frequency points. At resonance, the power transfer between the antenna and the source is maximized. In addition, the technique yields antennas that exhibit high tunability and can easily be loaded with active loads such as varactors. On the other hand, wideband yet electrically small antennas are very desirable for applications which require larger instantaneous bandwidth. In addition, such antennas can replace reconfigurable antennas, since there is no need to tune them. Again, the theory of CM can help to identify the type of active loads (Non-Foster Loads) required for widening both the input impedance bandwidth and the pattern bandwidth of electrically small antennas beyond the fundamental limit.

The theory of Characteristic Modes (CM) [8], [9] and [10] will be used to analyze small to mid-size antennas in order to broaden both the antenna pattern bandwidth and

the antenna input impedance bandwidth. This can be performed by carefully selecting the feeding locations and numbers of feed points. Furthermore, loading techniques based on the CM [11] and [12] can be used to design reconfigurable antennas with high tunability and acceptable VSWR. In addition to passive loading, active loading (i.e. non-Foster components) can result in a very wideband antenna if proper loads are chosen. Additionally, all the impedance bandwidths may be extended using matching networks, which are crucial components in the practical use of electrically small antennas.

Conventional passive matching networks have theoretical limitations on the maximum usable bandwidth they can achieve, as first stated by R.M. Fano [16]. On the other hand, active matching networks can exceed that fundamental limit and consequently open the door to practical, on-chip antenna designs. A theory of the design of active matching networks that implement non-Foster loads is required and is presented in the appendix. The appendices in this dissertation contain:

- Appendix A: Discussion on electrically small antenna (ESA) fundamental limitations.
- Appendix B: Discussion of the Q factor of the electrically small antennas and its impact on the antenna input impedance bandwidth.
- Appendix C: Discussion of the effect of passive matching networks on the antenna bandwidth.
- Appendix D: Discussion of matching network design using Real frequency Technique (RFT) [7].

1.2 Literature Review

The theory of Characteristic Modes was originally used to synthesize currents over the surface of both metallic and non-metallic scatterers to control their radar cross section (RCS). CM was also used to control the radiation pattern of an antenna [8][9] by modifying its shape or by loading it with lumped elements. Later on, there was some work on using the CM theory to determine the optimum location of an antenna on the surface of the supporting structure, i.e. airplane fuselage, vehicle body or mobile handset [42] [49] and [50]. Others used the CM theory as a tool to analyze antenna behavior by looking at its eigenvalues and eigenvectors. Very little work was done using the CM theory to design antennas, such as the work of a group in Spain where they have used the eigenvalue spectrum of a proximity coupled triangular patch to locate the frequency point at which two dominant modes (Horizontal and Vertical) have phase difference of 90^{o} to produce a circularly polarized radiation pattern [42].

In this work, the theory of Characteristic Modes is used to design broadband electrically small to mid size antennas that exhibit low Q factor over wide frequency bands which enable the use of matching network. The key idea is excite only one desired mode over the frequency band of interest by either modifying the antenna geometry or using loading.

1.3 Organization of the Dissertation

The organization of this dissertation is as follows. Chapter 2 discuses the design

methodology of small antennas using the theory of Characteristic Modes. The chapter starts describing the importance of the simultaneous design of the antenna and the matching network. Then, a discussion on design procedures of electrically small antennas by exciting one dominant mode over the desired frequency band will be discussed which should lead to an antenna with low Q factor and constant pattern shape over the desired frequency band. Finally, a brief discussion on the theory of Characteristic Modes will conclude this chapter.

In Chapter 3 a new model for the antenna's input impedance based of the theory of Characteristic Modes will be presented. The development of this model is a key contribution of this dissertation as it contributes to the understanding of the resonance phenomena of the input impedance of antennas. This model is extensively used in the successive chapters to design wideband small to mid size antennas. This chapter will also contain a discussion on the patch antenna's cavity modes and how Characteristic Modes are related to cavity modes.

Chapter 4 presents a bandwidth enhanced Vee shaped vertically polarized antenna which was designed based on the idea of exciting only one mode to obtain wide band input impedance and pattern behavior. The theory of Characteristic Modes was utilized in this chapter to help locate the optimum location of the feeds required to suppress the excitation of high order modes in the desired frequency band of operation. This chapter also discusses measured results of both input impedance and radiation pattern of two Vee antennas with different feed locations.

Chapter 5 discusses a design technique applicable to a reconfigurable antenna that is

based on the application of reactive loading. The load values are extracted using the theory of Characteristic Modes. This chapter also discusses the design of a reconfigurable dipole antenna and presents measured results of both input impedance and radiation pattern.

Chapter 6 discusses a design technique applicable for very wide band antenna based on the application of non-Foster reactive loading. The load values are extracted using the theory of Characteristic Modes. This chapter also discusses the design of a wide band dipole antenna and presents simulated results of both input impedance and radiation pattern.

Finally, in Chapter 7, the key contributions of this dissertation will be summarized and some suggestions for future work will be given as well.

CHAPTER 2

METHODOLOGY

A major goal of this work is to use the theory of characteristic modes with the theory of matching networks to increase both the input impedance bandwidth and the far field pattern bandwidth. For electrically small antennas, using a matching network is essential to broaden the antenna input impedance bandwidth since the real part of the input impedance is small while the reactive part is large. Thus, it is important when designing a small antenna (i.e. geometry, feed, etc …) to monitor the Q factor over the desired frequency range and to choose the antenna design which gives the lowest Q factor that also monotonically decreases over the desired frequency band. An oscillating behavior of the Q factor is an indication of high order mode excitation and thus it is undesirable. The following formula was used as a measure of the Q factor in the vicinity of series and parallel resonances [23]:

$$Q \approx \frac{\omega}{2R_{in}} \sqrt{\left(\frac{dR_{in}}{d\omega} \right)^2 + \left(\frac{dX_{in}}{d\omega} + \frac{\left| X_{in} \right|}{\omega} \right)^2} \tag{2.1}$$

where R_{in} and X_{in} are the antenna's frequency-dependent feed point resistance and reactance, respectively.

The theory of CM is used in several ways in this dissertation. First of all, it provides

physical insight into the behavior of any radiation structure when the CM and their corresponding eigenvalues and eigenpatterns are obtained. For example, the theory of CM is used to design the feeding network of antennas so the desired modes are excited while the undesired modes are not. The design methodology is summarized graphically in Figure 1. A brief discussion of the theory of CM is necessary to explain the new design methodology:

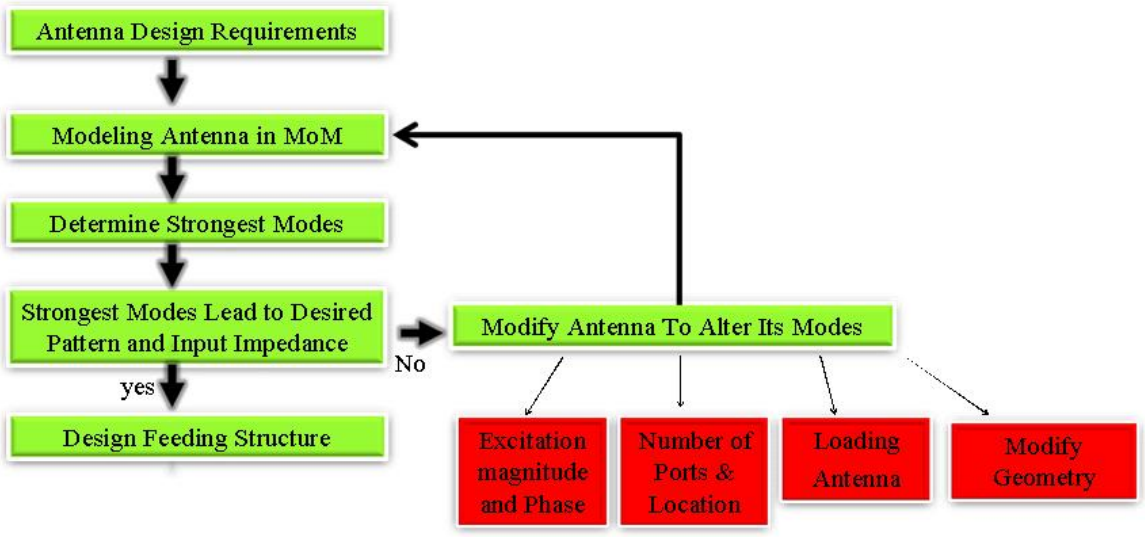

Figure 1 Flowchart of design methodology

The surface current $\vec{J}$ on the body of a lossless antenna can be written as a superposition of N weighted orthogonal current modes $\vec{J}_n$. In this discussion we will assume the body is made from a perfect electric conductor (PEC). The CM was also developed for dielectrics, but that formulation will not be discussed here. Each $\vec{J}_n$ has a corresponding eigenvalue λ_n; where both are functions of the antenna geometry. The

weighting coefficient of each mode $\vec{J}_n$ is a function of the eigenvalue λ_n and the inner product between the excitation voltage $\vec{E}^{in}$ and the current mode $\vec{J}_n$ as explained in the equation below:

$$\vec{J} = -\sum_{n}^{M} \alpha_n \vec{J}_n \tag{2.2}$$

$$\vec{J} = -\sum_{n}^{M} \frac{\left\langle \vec{J}_n, \vec{E}^{in}(\omega) \right\rangle}{1 + j\lambda_n(\omega)} \vec{J}_n \tag{2.3}$$

$\vec{J}_n$ and λ_n are solutions of the generalized eigenvalue equation shown below:

$$X\left(J_n\right) = \lambda_n R\left(J_n\right) \tag{2.4}$$

where X and R are the imaginary and real part of the Method of Moments (MoM) impedance matrix Z, respectively. Both X and R are real symmetric operators. Hence, all eigenvalues λ_n, and current modes $\vec{J}_n$ must be real. It is customary to normalize the eigencurrents such that $\left\langle R\vec{J}_n, \vec{J}_n \right\rangle = 1$. This normalization will be assumed in the rest of this dissertation.

To address the question of how the characteristic modes determine the antenna surface current we make use of the following observations: If the excitation vector $\vec{E}^{in}$ is orthogonal to the characteristic mode $\vec{J}_n$, the numerator of the coefficient α_n (the

inner product $\left\langle \vec{J}_n, \vec{E}^{in}(\omega) \right\rangle$) is equal to zero and thus that specific mode $\vec{J}_n$ will not be excited even if its corresponding λ_n in the denominator is equal to zero. On the other hand, if the magnitude of λ_n is very large, its corresponding characteristic mode $\vec{J}_n$ will have negligible effect on the antenna total current. Furthermore, when λ_n is zero, the corresponding characteristic mode $\vec{J}_n$ is referred to as a resonant mode. Based on these observations the desired modes can be excited while the undesired modes can be eliminated by applying the appropriate feed(s), loading, or/and geometry modifications to lower the antenna Q factor and to maintain the desired radiation pattern shape over the desired frequency band.

Although the theory of characteristic modes has historically been applied to the Method of Moments impedance matrix Z, it is also possible to apply it to a K-port network matrix N as in [11] such that equation (2.3) and (2.4) can be modified as follows:

$$\vec{J} = -\sum_{n}^{K} \frac{\left\langle \vec{J}_n, \vec{V}(\omega) \right\rangle}{1 + j\lambda_n(\omega)} \vec{J}_n \tag{2.5}$$

where $\vec{V}$ is the excitation voltage vector, $\vec{J}_n$ and λ_n are, respectively, solutions of the generalized eigenvalue equation shown below:

$$N_{\text{Im}}(J_n) = \lambda_n N_{\text{Re}}(J_n) \tag{2.6}$$

where N_{Im} and N_{Re} are the imaginary and real part of the open circuit Network matrix N, respectively. Both N_{Im} and N_{Re} are real operators. Hence, all eigenvalues λ_n, and current modes $\vec{J}_n$ must be real.

The K-port network CM is very useful when several feeding ports are used to excite an antenna and when loads are used at various port to modify the behavior of the antenna.

CHAPTER 3

DISCUSSION OF SERIES AND PARALLEL RESONANCE PHENOMENA IN THE INPUT IMPEDANCE OF ANTENNAS

3.1Introduction

The series and parallel resonances of an antenna's input impedance is explained through the theory of Characteristic Modes (CM). It is shown for the first time that parallel resonance phenomena corresponds to the interaction of at least two nearby CM, each having eigenvalues of opposite sign. Additionally, the series resonance phenomenon is shown to be mainly due to a single Characteristic Mode. Analysis of a simple wire dipole antenna and an edge fed patch antenna are used to validate this finding.

An antenna's input impedance is one of the most important parameters to assess its performance. It is therefore crucial to understand its behavior as a function of frequency, size, materials, etc. This knowledge can be used to optimize the performance of antennas in many applications, such as broadening the bandwidth of an electrically small antenna [38], [39] and [37]. Although lumped circuit models have generally been used to represent the frequency behavior of the input impedance, an alternative approach that should lead to more physical insight into the antenna performance is presented here

based on the theory of Characteristic Modes.

The input impedance *Z* of an antenna near series resonance can be modeled as a lumped series *RLC* circuit, namely,

$$Z = R_s + j\left(\omega L_s - \frac{1}{\omega C_s}\right) \tag{3.1}$$

At resonance ω_s, the imaginary parts of the series impedances cancel each other, where $\omega_s = \sqrt{1/L_s C_s}$. Consequently, only the real part of the *RLC* circuit contributes to the antenna input impedance. Also, note that the derivative of the reactance with respect to frequency is positive at that series resonance. On the other hand, near a parallel resonance, the antenna input admittance *Y* can be modeled as lumped parallel *RLC* circuit:

$$Y = \frac{1}{R_P} + j\left(\omega C_P - \frac{1}{\omega L_P}\right) \tag{3.2}$$

At resonance ω_p, the imaginary parts of the parallel admittances cancel each other, where $\omega_p = \sqrt{1/L_p C_p}$. Consequently, only the real part of the RLC circuit contributes to the antenna input impedance. In this case, the derivative of the susceptance with respect to frequency is positive at resonance. For an applied voltage V_{in} at the feed point (Fixed Voltage Value), the value of the input impedance (V_{in}/I_{in}) at the antenna feed port

depends on the antenna current I_{in} flowing into the feed port. Hence, the antenna resonance behavior will be studied by analyzing the antenna current behavior at the feed port.

Series resonance at the antenna input port occurs when the current at the port reaches its greatest effective value, while the opposite occurs during parallel resonance. However, for some antennas, the behavior of the input impedance near parallel resonance is more complicated than the model used in equation (3.2). For example, a probe-fed microstrip antenna has a non-zero reactance when the real part is maximum, resulting in a current minimum at a frequency that is slightly shifted from the frequency where the real part of the input impedance is maximum. In both cases, the voltage V_{in} across the input port is in phase with the current I_{in}. As will be explained in this chapter, series resonance is a "natural" resonance; namely, it occurs at the resonances of the Characteristic Modes (CM). On the other hand, parallel resonance is the result of the interaction of two or more CM.

In this chapter, the resonances of the input impedance of three antenna structures; namely, a center fed dipole antenna, an edge fed Microstrip patch antenna and a loop antenna will be discussed. The conceptual framework of this discussion relies heavily upon the theory of Characteristic Modes [8],[9] and [10] discussed in Chapter 2 and briefly presented here.

3.2 THEORY OF CHARACTERISTIC MODES

The surface current density $\vec{J}$ on the body of a lossless metallic antenna can be

written as a superposition of N weighted orthogonal current modes $\vec{J}_n$. Each $\vec{J}_n$ corresponds to an eigenvalue λ_n; where both components of an eigenpair are functions of the antenna geometry. The weighting coefficient of each mode is function of both; the mode's corresponding eigenvalue λ_n and the inner product of that mode with the excitation vector $\vec{E}^{in}$ as explained in the equation below:

$$\vec{J}(\vec{r},\omega) = \sum_n \frac{\left\langle \vec{J}_n(\vec{r},\omega), \vec{E}^{in}(\vec{r},\omega) \right\rangle}{(1+j\lambda_n(\omega))\left\langle R\vec{J}_n(\vec{r},\omega), \vec{J}_n(\vec{r},\omega) \right\rangle} \vec{J}_n(\vec{r},\omega) \tag{3.3}$$

The inner product is defined on the surface of the antenna as follows:

$$\left\langle \vec{a}, \vec{b} \right\rangle = \int_S \vec{a}^* . \vec{b}\, ds \tag{3.4}$$

where $\vec{J}_n$ and λ_n are the solutions of the generalized eigenvalue equation shown below:

$$X(J_n) = \lambda_n R(J_n) \tag{3.5}$$

where *X* and *R* are the imaginary and real part of the MoM ingteraction impedance matrix *Z*, respectively.

3.3 Center Fed Dipole Antenna

The first three dominant Characteristic Modes of a wire dipole antenna are shown in Figure 2. Modes 1 and 3 are even modes while Mode 2 is an odd mode with a null at the center of the dipole. In the case of a center fed dipole antenna, odd modes will not be

excited since the inner product $\left\langle \vec{J}_n(\omega), \vec{E}^{in}(\omega) \right\rangle$ in Equation (3.3) will equal to zero; hence, only the even modes will be considered in this example.

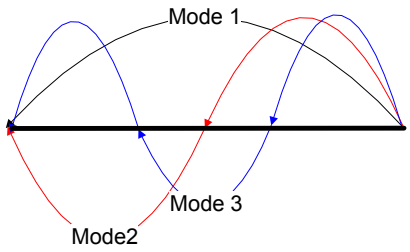

Figure 2 First three dominant modes of a dipole antenna

The input impedance of a center fed 1.2 m length wire dipole antenna simulated using ESP5 [24] is shown in Figure 3. It is apparent that two series resonances occur in the frequency range 20 MHz to 400 MHz. The first resonant frequency occurs at 119.5 MHz, while the second resonant frequency occurs at 367.5 MHz. Between these two series resonances is one parallel resonance that occurs at 222 MHz.

To understand the occurrence of the two series resonances in terms of the dipole Characteristic Modes, a plot of the dipole weight function spectrum is shown Figure 4. As can be seen in the graph, λ_1, which corresponds to the first dipole mode, is equal to zero at 119.5 MHz, while λ_3, which corresponds to the third dipole mode, is equal to zero at 367.5 MHz. Those two frequencies, for which the eigenvalues λ_n are equal to zero, also correspond to the series resonance frequencies of the antenna input impedance.

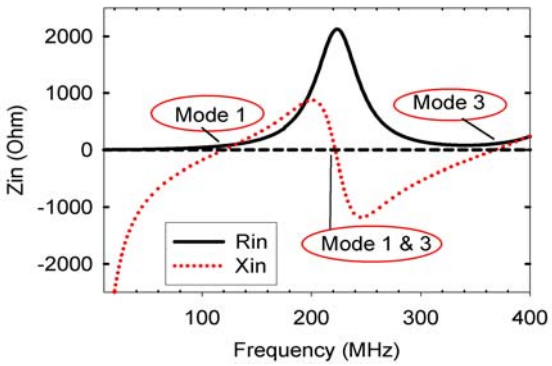

Figure 3 Input impedance of a center fed dipole antenna

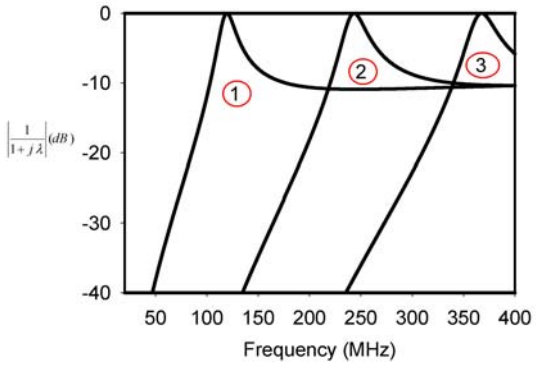

Figure 4 Weight function spectrum of the dipole antenna

The input impedance of the antenna is equal to the voltage across the input port at $\vec{r}_o$ divided by the current at the same port, namely, $Z_{in} = V^{in}(\vec{r}_o)/I(\vec{r}_o)$. Near the first series resonance, the total surface current at the input port $\vec{r}_o$ can be written as

$$\vec{J}(\vec{r}_o) = \frac{J_1^*(\vec{r}_o)E^{in}(\vec{r}_o)}{1+j\lambda_1}\vec{J}_1(\vec{r}_o) + HOT \tag{3.6}$$

where it is assumed Mode 1 is dominant because it is near its resonance ($\lambda_1 \approx 0$) and "HOT stands for "higher order terms". Following common practice, the excitation vector $\vec{E}^{in}$ is assumed to be highly localized, namely, it can be safely approximated to be zero almost

everywhere except at the feed port. Assuming the input feed port is Δl in length and Δw in width, the input impedance can be written as follows:

$$Z_{in} = \frac{V^{in}(\vec{r}_o)}{I(\vec{r}_o)} = \frac{E^{in}(\vec{r}_o)\Delta l}{J(\vec{r}_o)\Delta w} = \frac{E^{in}(\vec{r}_o)\left(1+j\lambda_1\right)\Delta l}{J_1^*(\vec{r}_o)E^{in}(\vec{r}_o)J_1(\vec{r}_o)\Delta w} + HOT$$
$$= \frac{\Delta l}{|\vec{J}_1(\vec{r}_o)|^2\,\Delta w} + j\,\frac{\lambda_1 \Delta l}{|\vec{J}_1(\vec{r}_o)|^2\,\Delta w} + HOT \tag{3.7}$$

Thus, the input impedance will be purely resistive in the case of series resonance when λ_1 approaches zero (Mode 1 resonates). Furthermore, since the magnitudes of the remaining eigenvalues are relatively very large, their corresponding modes will be weakly excited and will have negligible contribution to the total current and the input impedance.

The same analysis applies to degenerate systems where two or more eigenvalues approach zero at the same frequency. Hence, the summation of terms from Equation (3.3) will still have the same phase as the excitation vector $\vec{E}^{in}$. In some cases, more than one higher order mode may be strongly excited along with the dominant mode. If those higher order modes have relatively small eigenvalue magnitudes compared to the dominant mode n when λ_n is equal to zero, then the n^{th} term will not be the only term in the summation. Therefore, the phase of the total current will not be the same as the phase of excitation vector $\vec{E}^{in}$. Consequently, the zero-crossing frequency of the input reactance will either shift or the reactance may not have a zero-crossing at all.

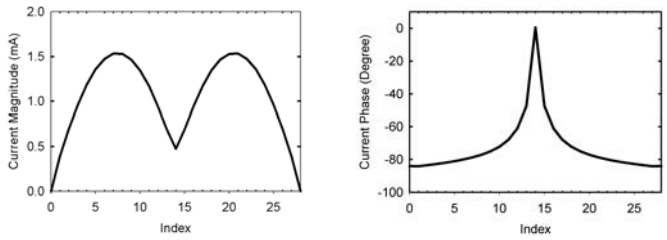

Figure 5 Current magnitude and phase distribution along the dipole antenna at parallel resonance

To explain the parallel resonance of the center fed dipole using the dipole Characteristic Modes, it is necessary to understand what happens to the current at the feed port. At parallel resonance, the current at the feed port approaches zero magnitude and zero phase, as shown in Figure 5 (Not exactly zero due to contribution of high order modes). The current distribution in this graph illustrates that the current along the center fed dipole antenna becomes small at the center of the dipole antenna. However, this cannot be due to a single mode because any current mode with null at the feed port will not be excited, since the inner product in the numerator of Equation (3.3) $\left\langle \vec{J}_n(\vec{r},\omega), \vec{E}^{in}(\vec{r},\omega) \right\rangle$ would be zero.

Thus, in the case of a parallel resonance, there should be at least two strongly, but equally, excited modes with opposite phase at the input port in order to cancel each other at this port. We conclude that there is no single Characteristic Mode called a parallel mode, since this type of resonance should be an interaction of at least two nearby series modes with opposite sign. Therefore, parallel resonance is a function of two factors: the feed location (inner product in numerator of Equation (3.3)), and the antenna geometry.

Since at parallel resonance the current is composed of at least two dominant modes,

the total current $\vec{J}$ along the antenna body can be written in the neighborhood of the parallel resonance frequency as follows (assuming two dominant terms):

$$\vec{J} = (1 - j\lambda_1)\frac{\langle \vec{J}_1, \vec{E}^{in} \rangle}{1+\lambda_1^2}\vec{J}_1(\vec{r}) + (1 - j\lambda_3)\frac{\langle \vec{J}_3, \vec{E}^{in} \rangle}{1+\lambda_3^2}\vec{J}_3(\vec{r}) + \text{HOT} \tag{3.8}$$

At the feed port $\vec{r}_o$, Equation (3.8) may be written as:

$$\vec{J}(\vec{r}_o) = (1 - j\lambda_1)\frac{J_1^*(\vec{r}_o)E^{in}(\vec{r}_o)}{1+\lambda_1^2}\vec{J}_1(\vec{r}_o) + (1 - j\lambda_3)\frac{J_3^*(\vec{r}_o)E^{in}(\vec{r}_o)}{1+\lambda_3^2}\vec{J}_3(\vec{r}_o) + \text{HOT} \tag{3.9}$$

The antenna admittance due to the two strongly excited modes can be written as follows, near the parallel resonance frequency:

$$Y = \frac{I(\vec{r}_o)}{V^{in}(\vec{r}_o)} = \frac{J(\vec{r}_o)\Delta w}{E^{in}(\vec{r}_o)\Delta l} = (1 - j\lambda_1)\frac{|\vec{J}_1(\vec{r}_o)|^2\,\Delta w}{(1+\lambda_1^2)\Delta l} + (1 - j\lambda_3)\frac{|\vec{J}_3(\vec{r}_o)|^2\,\Delta w}{(1+\lambda_3^2)\Delta l} + \text{HOT} \tag{3.10}$$

Since both λ_1 and λ_3 magnitude are much larger than 1 and have opposite signs:

$$\text{Re}(Y) = \frac{\Delta w}{\Delta l}\left(\frac{|\vec{J}_1(\vec{r}_o)|^2}{\lambda_1^2} + \frac{|\vec{J}_3(\vec{r}_o)|^2}{\lambda_3^2}\right) + \text{HOT} \tag{3.11}$$

$$\left|\text{Im}(Y)\right| = \frac{\Delta w}{\Delta l}\left(\left|\frac{|\vec{J}_1(\vec{r}_o)|^2}{|\lambda_1|} - \frac{|\vec{J}_3(\vec{r}_o)^2|}{|\lambda_3|}\right|\right) + HOT \tag{3.12}$$

Hence when:

$$\left|\frac{\vec{J}_1(\vec{r}_o)^2}{\lambda_1}\right| = \left|\frac{\vec{J}_3(\vec{r}_o)^2}{\lambda_3}\right| \tag{3.13}$$

the imaginary part of the admittance approaches zero while its real part is small because the magnitude of the eigenvalues is large. In other words, the real part of the input impedance becomes large and the imaginary part approaches zero (and changes sign) at parallel resonance.

3.4 Edge Fed Rectangular Microstrip Patch Antenna

3.4.1 Resonances

A rectangular edge fed Microstrip patch antenna, 16 mm x 12.448 mm in size, and mounted on a 31 mil substrate with dielectric constant of 2.2 is shown in Figure 6. The input impedance simulated using FEKO [40] is shown in Figure 7. As can be observed, the first parallel resonance occurs at 6.1 GHz between two series resonances: one at 2.2 GHz and a second one at 6.9 GHz. As shown in Figure 8, the first series resonance is due to Mode 1 and occurs at the frequency at which the eigenvalue of Mode 1 approaches zero. Similarly, the second series resonance occurs at the frequency at which the eigenvalue of Mode 2 approaches zero. Note that the first series resonance (Mode 1) occurs when the L-shaped length of the current path on the patch (see Figure 6 (b)) plus its image (ground plane) is approximately $\lambda/2$ at 2.2 GHz, where λ is the wavelength in a medium with a dielectric constant equal to the effective dielectric constant of the

structure ($\varepsilon_{r,eff}$=1.8). Using this length makes sense because when the feed point is near the corner, the currents for Mode 1 tend to flow in that direction at 2.2 GHz. It can be shown that the frequency at the first series resonance increases if the feed point is moved towards the center of the edge. This also makes sense because the effective length decreases, since the currents of Mode 1 for this feed point location (near center of edge) tend to flow parallel to the long edge of the patch. Furthermore, Mode 1 does not radiate well because the current on the patch and its image on the ground plane tend to cancel each other.

Previous work [41] and [42] on determining the Characteristic Modes of a patch antenna was done by ignoring the feeding structure of the antenna and treating the patch antenna as a plate parallel to the ground plane. This treatment yields different Characteristic Modes than an actual patch antenna. For an actual patch antenna, the feed structure connects the top plate to the ground plane physically either through coaxial feed or Microstrip feed, which is a different geometry than just two parallel plates without feeding structure. There are also Microstrip patch antennas that are fed through proximity coupling [43], but the feeding structure (e.g., hole in the ground plane) has to be modeled as well. Otherwise, different Characteristic Modes are obtained.

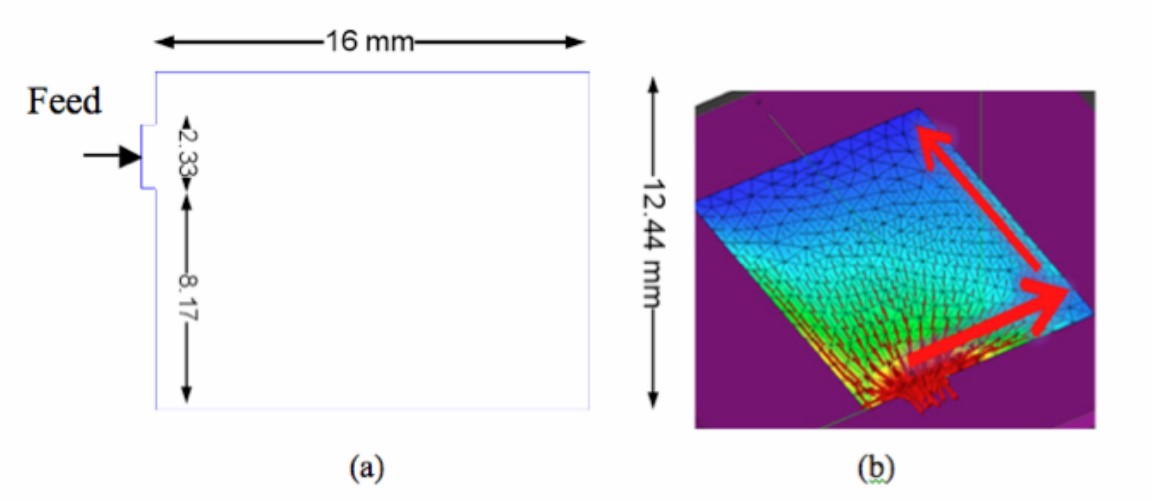

Figure 6 Edge fed patch antenna (dimensions in mm)

The current magnitudes of Mode 1, Mode 2, and the total current at the input port, which consists mostly of a summation of the two dominant modes(Mode 1 and Mode 2), are shown in Figure 9. Clearly, the current magnitude of Mode 1 approaches its maximum at the frequency which corresponds to the first series resonance. Similarly, Mode 2's maximum occurs at the frequency which corresponds to the second series resonance. On the other hand, the parallel resonance at 6.1 GHz is due to current cancellation at the input port between Modes 1 and 2, since both modes have similar magnitude (Figure 9) but opposite phase at the input port (Figure 10).

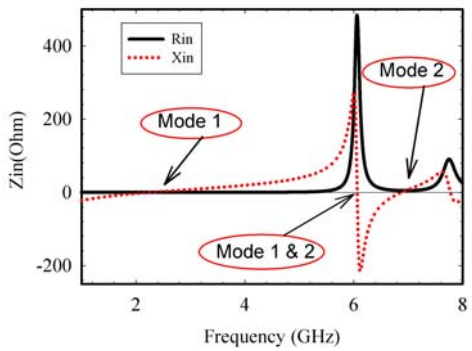

Figure 7 Input impedance of the patch antenna

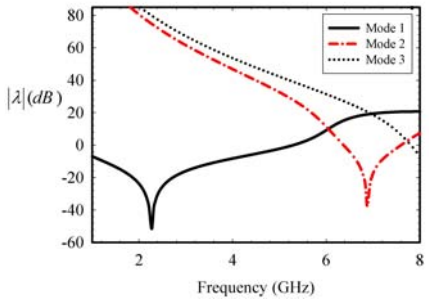

Figure 8 Eigenvalue spectrum of the patch antenna

3.4.2 Current Distribution

The magnitude of the normalized total current distribution of the Microstrip patch antenna at the first three resonant frequencies is shown in Figure 13. As can be seen, the normalized current distribution at the first and the second series resonances is very small everywhere along the patch surface except at the input port. In contrast, at parallel resonance, the current distribution along the patch antenna surface is similar to the well known cavity mode TM_{01}. Thus, the patch antenna is a poor radiator at its series resonances and a good radiator at its parallel resonance.

Figure 14 and Figure 15 show, respectively, the magnitude of the normalized current distribution of mode 1 and 2 at the first three Microstrip patch resonances; namely, 2.2 GHz, 6.1 GHz and 6.9 GHz. As can be seen in the graph, at 2.2 GHz, where λ_1 approaches zero, the current distribution of Mode 1 is similar to the normalized patch total current distribution at 2.2 GHz (Figure 13). Also, the normalized current distribution of Mode 2 (Figure 15) at 6.9 GHz, where λ_2 approaches zero, is similar to the normalized total current distribution at 6.9 GHz (Figure 13). This behavior is expected since the total

current distribution at a series resonance is mainly due to the contribution of the sole dominant Characteristic Mode.

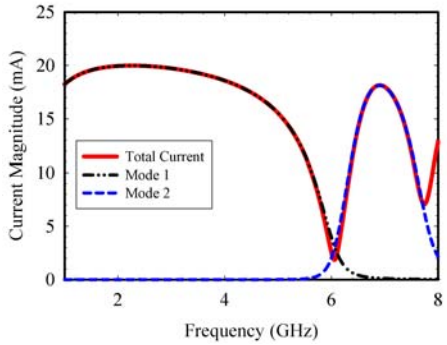

Figure 9 Current magnitude at the input port of the edge fed patch antenna

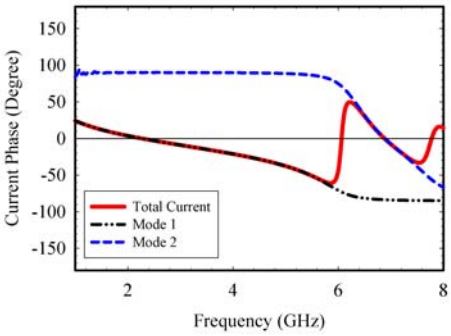

Figure 10 Phase of currents at the input port of the edge fed patch antenna

At 6.1 GHz, since both Modes 1 and 2 are dominant modes and both have similar normalized current magnitudes distributions and phase, the total normalized current distribution resembles these modes, except in the vicinity of the input port where the these two currents are out of phase.

3.4.3 Cavity Modes versus Characteristic Modes

Microstrip patch antennas are generally narrowband antennas operated at

frequencies corresponding to their lowest order cavity modes. However, away from the resonant frequencies of the cavity modes, Microstrip patch antennas are poor radiators. The Microstrip patch antenna under discussion has its first cavity mode at 6.1 GHz (Figure 13) which corresponds to the first parallel resonance of its input impedance. Hence, we conclude that the Characteristic Modes do not correspond to the cavity modes, but rather cavity modes correspond to the patch parallel resonances, which is an interaction of two nearby Characteristic Modes.

3.5 Circular Loop Antenna

This circular loop antenna is considered here because it has a somewhat different behavior compared to the dipole antenna. The former is a closed structure, while the latter is open. In other words, a current can flow in the loop antenna even at zero frequency (DC current), while that is physically impossible in the dipole antenna. This has an important implication in the behavior of the input impedance of the antenna. The imaginary part of the input impedance of a 3 cm radius circular loop antenna is shown Figure 11. The first parallel resonance of this loop antenna occurs around 0.744 GHz. Figure 12 shows the eigenvalue spectrum of the loop antenna. Note that because of the antenna symmetry, degenerate modes will exist. Furthermore, there is a conductive mode (Mode 0) that resonates at zero Hz. Hence, the first parallel resonance of the loop antenna is due to the interaction of the degenerate Modes 1 and 2 with Mode 0.

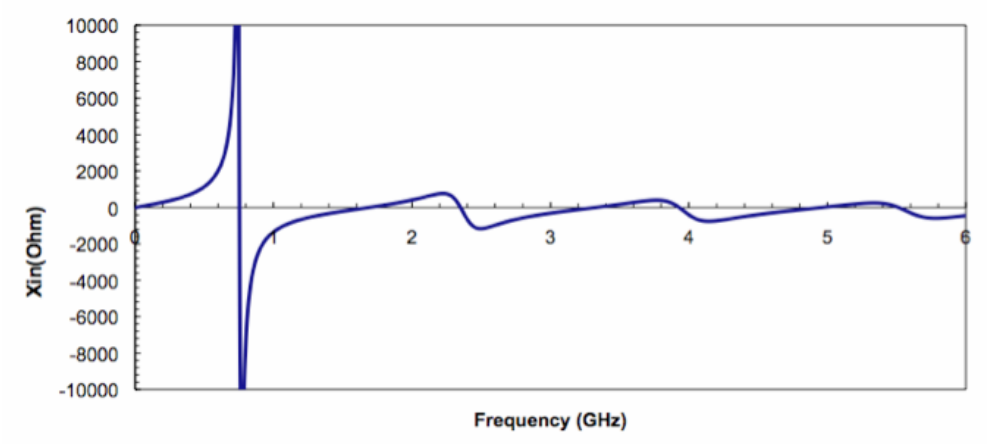

Figure 11 Imaginary part of the input impedance of the 3 cm radius circular loop antenna

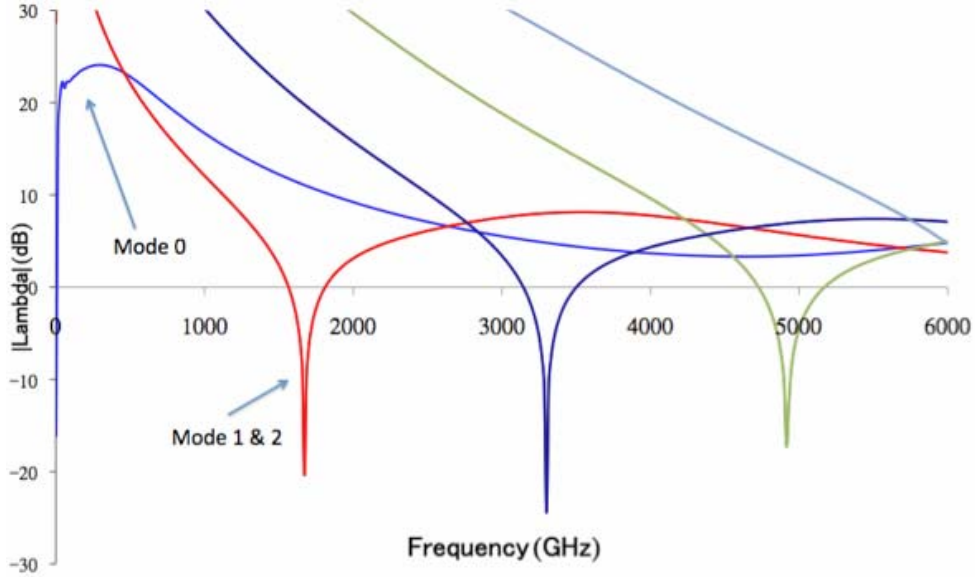

Figure 12 Eigenvalue spectrum of the loop antenna

3.6 Conclusion

The theory of Characteristic Modes was used to model the input impedance of various antennas in terms of its modes. It was shown that parallel resonance phenomena does not correspond to a single Characteristic Mode, but is rather due to an interaction of mainly two nearby modes each having eigenvalues of opposite sign. This is in contrast to

the series resonance phenomenon, which is mainly due to a single resonant Characteristic Mode (when corresponding eigenvalue becomes zero). It was also shown that the Characteristic Modes of a microstrip patch antenna do not correspond to its cavity modes. This explains why the microstrip antenna normally operates at parallel resonance since the cavity mode can be expressed as the combination of at least two Characteristic Modes. A loop antenna was the third antenna modeled here. This antenna has a DC mode which is not the case for the dipole or microstrip patch antennas. Although we only considered three different types of antennas, we believe for any antenna, series resonance in the input impedance is due to the resonance of its Characteristic Modes while parallel resonance is due to the interaction of two or more Characteristic Modes.

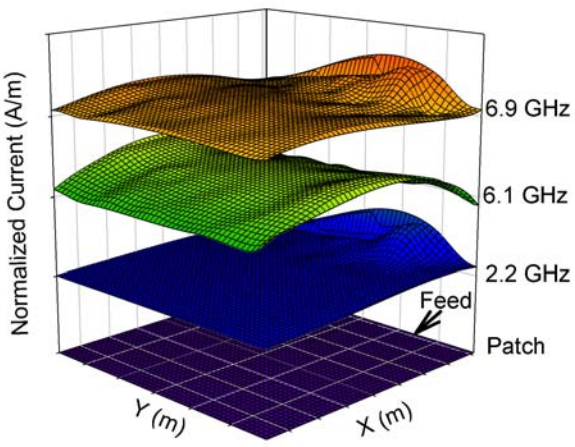

Figure 13 Total current distribution of the patch antenna at its first three resonances: (series resonances at 2.2 GHz & 6.9 GHz) and parallel resonance at 6.1 GHz

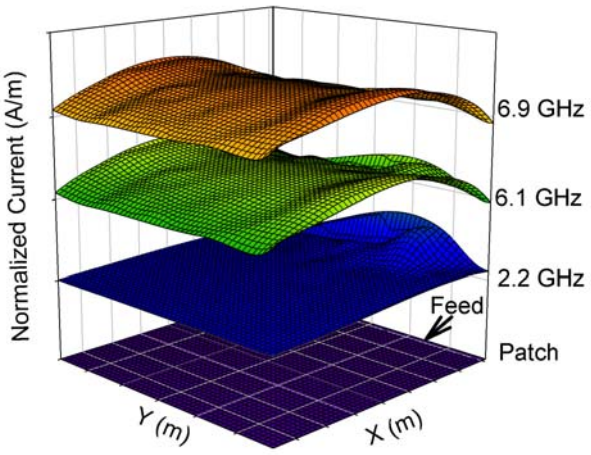

Figure 14 Mode 1 current distribution of the patch antenna at its corresponding three resonances (series resonance: 2.2 GHz & 6.9 GHz) and parallel resonance at 6.1 GHz

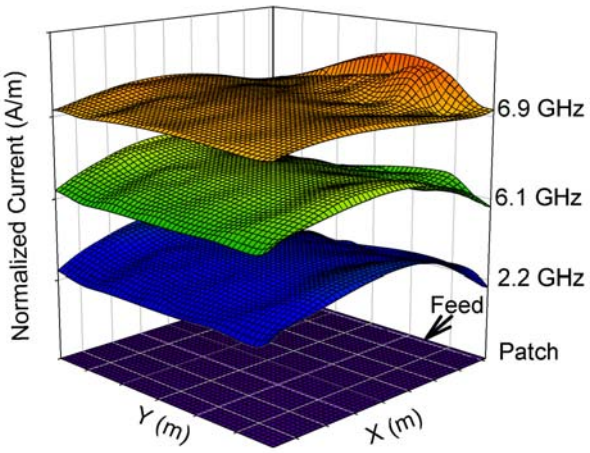

Figure 15 Mode 2 current distribution of the patch antenna at its corresponding three resonances (series resonances at 2.2 GHz & 6.9 GHz) and parallel resonance at 6.1 GHz

CHAPTER 4

VERTICALLY POLARIZED VEE ANTENNA

4.1 Introduction

The goal of this chapter is to design a conformal vertical polarized antenna with reasonable bandwidth for the Manta UAV (Figure 16). It is a challenging example because the antenna has to be conformal to the V shaped tail of the UAV; however, it has to radiate a vertically polarized Omni-Directional pattern in the frequency range from 50 to 90 MHz. To obtain this vertical polarized radiation over larger frequency bandwidth a long enough vertical part of the Manta should be used. As can be seen in Figure 16 the Manta longest vertical physical length is its V-Tail (Ruddervator), λ/17 at 50 MHz. The V-Tail looks like an inverted Vee antenna, similar to the well known Vee antenna. However, to achieve the desired pattern and polarization, the antenna should be excited at two locations with two out of phase sources as shown in Figure 17.

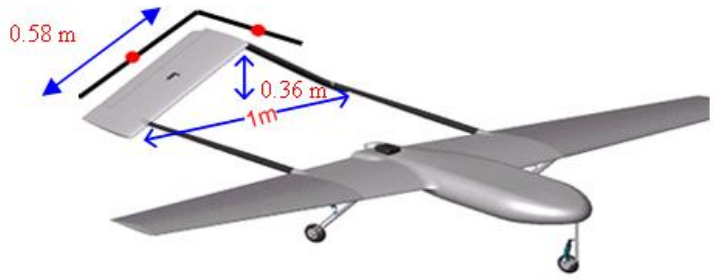

Figure 16 Manta (UAV)

The Vee Antenna can be analyzed using the Characteristic Mode theory (CM) in order to optimally design the excitation scheme. A thin Vee shape wire dipole was considered first; from the CM analysis, the first three dominant modes are shown in Figure 18. It is clear that Mode 2 is the desired mode at which each arm has the same current magnitude but with opposite direction. Mode 2 current can be decomposed into two components, vertical and horizontal components as shown in Figure 19. The horizontal components consist of two currents that oppositely directed which will produce a small horizontal far field. On the other hand the vertical components consist of two in-phase vertical currents which will produce the desired omnidirectional vertically polarized far field.

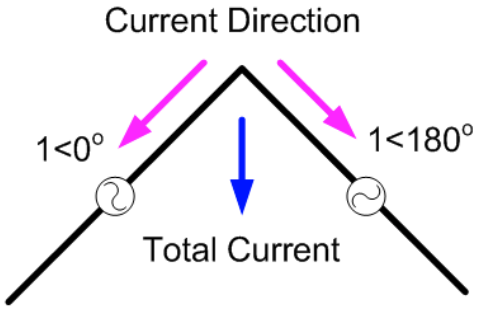

Figure 17 Vee Antenna Fed With Two Out Of Phase Sources

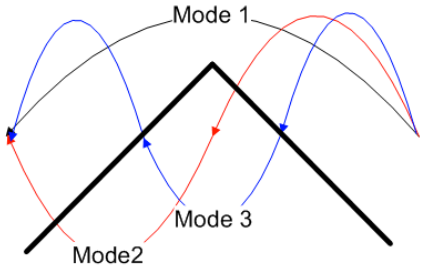

Figure 18 The First Three Dominate Modes On The Vee Antenna

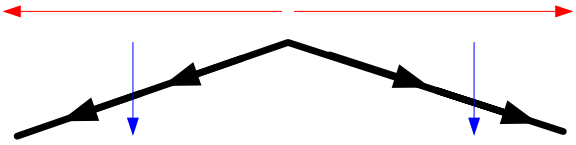

Figure 19 Vertical And Horizontal Projection Of The Current On The Vee Antenna

In order to excite Mode 2, the source can not be placed on the center of the Vee Antenna (apex) since this mode has a null at the middle (will not be excited). A good place for the source will be at the center of either arm or at the null of the third mode such that the third mode will not be excited as well. However, installing one source at either arm will excite the undesired Mode 1 (in addition to Mode 2). Instead, two out of phase sources at each arm can be used to eliminate even modes (i. e. Mode 1 & Mode 3) as shown in Figure 20 and Figure 21.

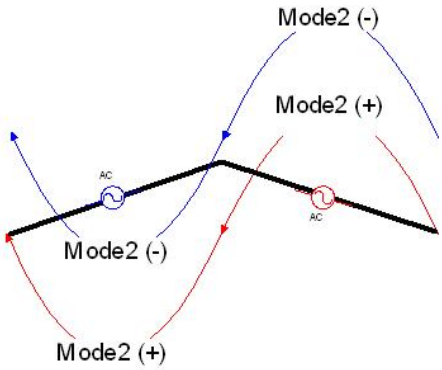

Figure 20 Two Out Of Phase Sources On The Vee Antenna Establish The Second Mode

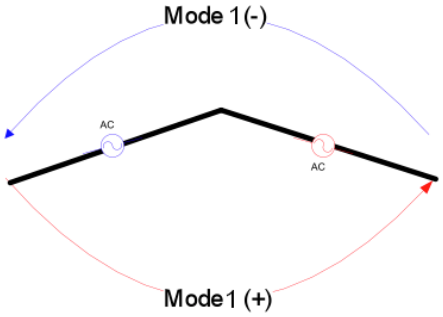

Figure 21 Two Out Of Phase Sources On The Vee Antenna Cancel The Even Mode (First Mode)

4.2 Meander Vee Antenna

A Bowtie conformal to the V shape structure was first evaluated versus a conformal

meander line antenna. Since the structure size is very small the Bowtie produced a very high Q factor. Thus a meander line antenna was chosen for the Manta in order to mitigate the effect of the high capacitive reactance of the input impedance of an electrically small Vee antenna (Figure 22). The Q factor of the input impedance was calculated at the feeding port of an ideal 3 dB Hybrid coupler which is connected to the two ports of the Meander Antenna using [17]:

$$Q \approx \frac{\omega}{2R_{in}} \sqrt{\left(\frac{dR_{in}}{d\omega}\right)^2 + \left(\frac{dX_{in}}{d\omega} + \frac{|X_{in}|}{\omega}\right)^2} \tag{4.1}$$

where R_{in} and X_{in} are the antenna's frequency-dependent feed point resistance and reactance, respectively.

A 21-element meander line antenna was chosen after evaluating type of antenna with different number of elements in order to decide on the optimum number that gives the lowest Q factor over the desired bandwidth (see Figure 23).

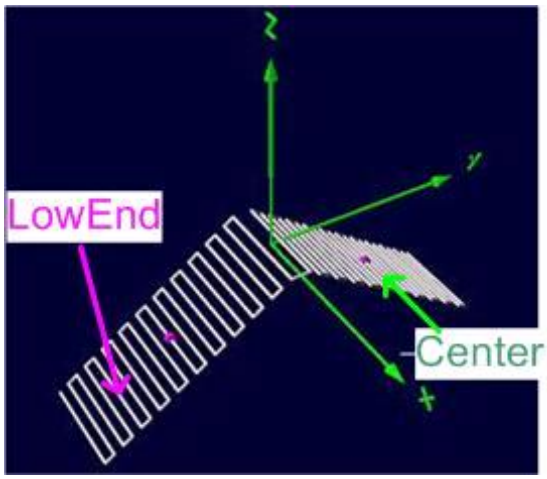

Figure 22 Meander line Vee antenna with two sets of potential feed locations

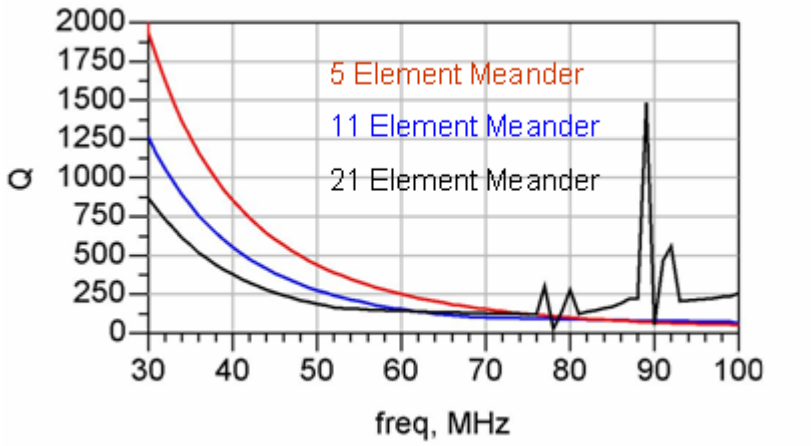

Figure 23 Q factor of 5 element, 11 element and 21 elements Meander line antennas

4.3 Optimum Port Location on Each Arm of the Meander

To obtain wider gain bandwidth, the proper location of the sources on each arm is critical to eliminate the excitation of the stronger high order odd modes in the desired frequency band. High order mode excitations alongside the desired dominant mode can degrade the Q factor of the antenna and consequently the ability to design wideband matching network. The plot in Figure 24 shows the spectrum of $\left|\frac{1}{1+j\,\lambda_n(\omega)}\right|$ of the first

three odd modes; the mode labeled as 2 is the desired odd mode.

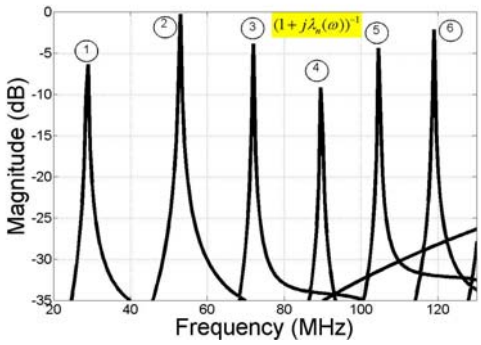

Figure 24 Weight Function Spectrum of a Vee Shape Antenna

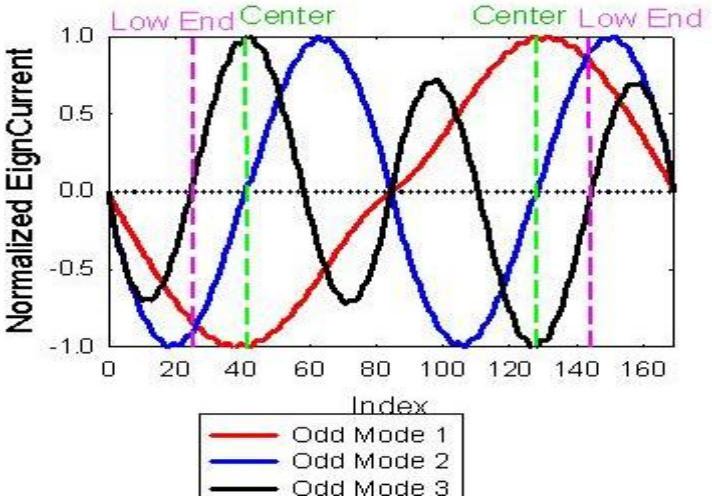

Figure 25 Current Distribution of the first three odd modes along the Meander Antenna

Making use of the fact that placing a source at the null of an eigenmode will not excite that specific mode, that is, the numerator of equation $\left\langle \vec{J}_n(\omega), \vec{E}^{in}(\omega) \right\rangle$ become zero, high order odd modes can be eliminated by choosing the proper source location at each arm. Plots of the current distribution of the first three odd modes as shown in Figure 25 indicates that the second odd mode has its null at the center of each arm while the third odd mode has its null toward the low end of each arm. Hence, the proper location of the source is at the center of each arm.

4.4 Simulated Results

It is clear from the plot of the imaginary part of the input impedance shown in Figure 26 that both feeding locations have their series resonance occur at the same frequency point (where $\lambda_2 = 0$) since eigenvalues are only a function of geometry. However, since parallel resonance is a function of feeding and geometry, the parallel resonance for the case of the center feed excitation occurs at a high frequency point compared to the case of the low end excitation. Consequently, as shown in Figure 28, center fed antenna has the potential to lower the Q in the desired frequency band.

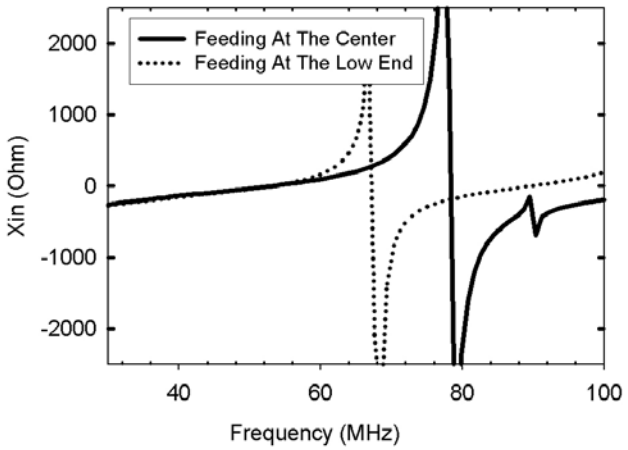

Figure 26 Imaginary part of the input impedance of the 21-elemnt Meander Antenna (Center Feed vs. Low End Feed)

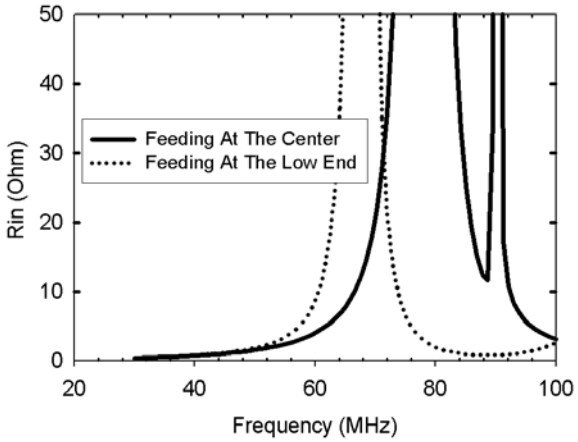

Figure 27 The Real part of the input impedance of the 21-elemnt Meander Antenna (Center Feed vs. Low End Feed)

The 3D radiation pattern of the center fed excitation (Figure 29) gives the desired omni-directional pattern up to 110 MHz while for the low end excitation case (Figure 30) the antenna has omni-directional behavior only up 85 MHz, clearly due to the early high order mode excitation. Although the 110 MHz frequency is higher than the band of interest, it is shown here to demonstrate that it is still omni-directional even at this frequency where there is a risk of exciting higher order modes. That is another advantage of the CM theory. The cross polarized component is not shown here, but it is around -11dB below the vertical component gain.

The lower Q factor of the center fed case result in better matching network design as can be seen in Figure 35, the absolute gain (vertical polarization) of the antenna without a matching network is shown in dashed line. Solid line in Figure 35 shows the performance of the antenna with 7th order lossless matching network with discrete elements (capacitors and inductors) designed using Real Frequency Technique (RFT) [25].

On the other hand, the matching network in the low end excitation case did not

provide remarkable enhancement because both the Q factor and the pattern behavior were degraded due to the presence of high order modes at the high frequency end.

Finally, Figure 31 & Figure 32 shows a comparison of the absolute vertical/horizontal gain between the two cases, center fed excitation and low end excitation when a matching network is used. It can be seen that a gain of around -11dB is obtained in the frequency range from 50 to 90 MHz. Obviously the matching network yields a better performance over the band of interest. On the other hand, Figure 33 & Figure 34 show the vertical/horizontal gain, without matching network, for the same two cases, namely center fed excitation and low end excitation.

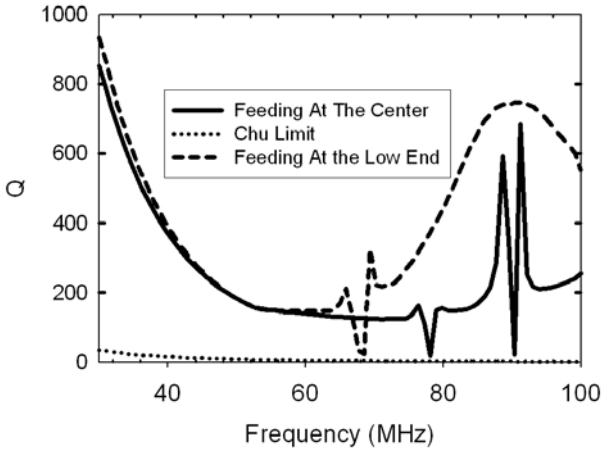

Figure 28 The Q of the input impedance of the 21-elemnt Meander Antenna (Center Feed vs. Low End Feed)

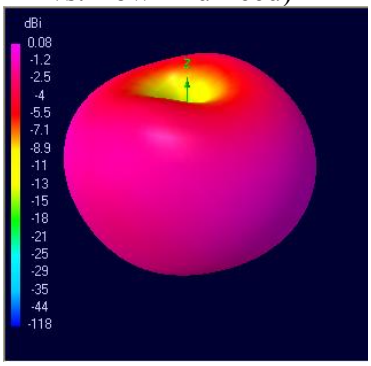

Figure 29 Vertically polarized radiation pattern at 110 MHz, center fed case

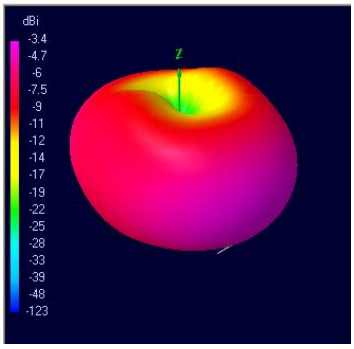

Figure 30 Vertically polarized radiation pattern at 85 MHz, Low end fed case

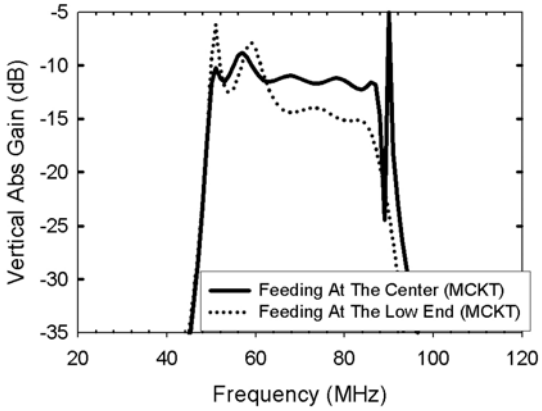

Figure 31 Realized Vertical Gain with Matching Network Circuit (MCKT), center fed excitation, vs. low end excitation.

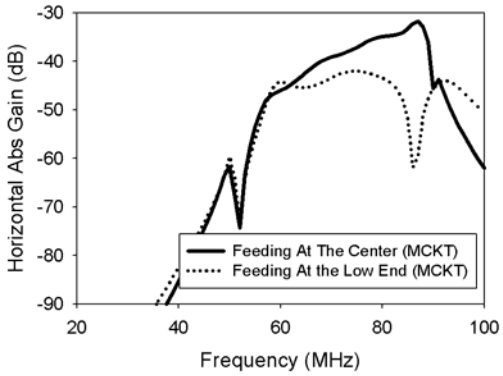

Figure 32 Realized Horizontal Gain with Matching Network Circuit (MCKT), center fed excitation, vs. low end excitation.

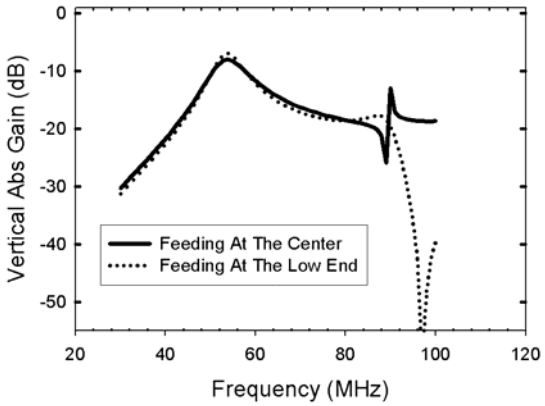

Figure 33 Realized Vertical Gain, center fed excitation, vs. low end excitation.

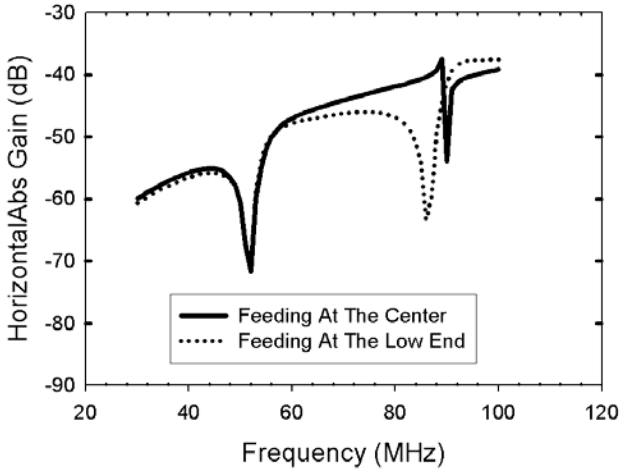

Figure 34 Realized Horizontal Gain, center fed excitation, vs. low end excitation.

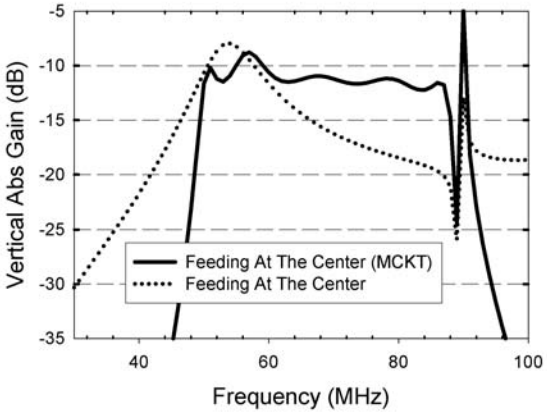

Figure 35 Realized Vertical Gain of the center fed excitation case, Matching Network Circuit (MCKT) vs. none.

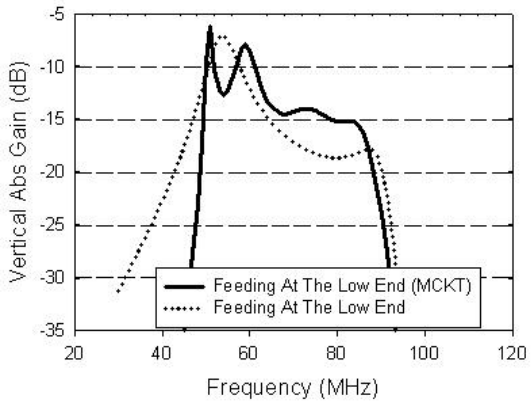

Figure 36 Realized Vertical Gain of the low end fed excitation case, Matching Network Circuit (MCKT) vs. none

4.5 Measured Results

Figure 37 shows the meander line antenna built using 6mm wide copper tape and mounted on 3cm thick Vee shaped foam of dielectric constant (Єr) equal to 1.3. The size of each arm is 0.62 m by 0.25 m. Each meander arm is fed using ZFSCJ-2-1-S (Mini-Circuits) balun through two 0.44 m coaxial cables at each balun port. A power divider ZFSCJ-2-1-S+ (Mini-Circuits) is used to feed the two baluns through two 0.44 m coaxial cables. Figure 38 and Figure 39 show the measured real and imaginary parts of the input impedance at the input port of the power divider for the two feeding schemes, the Center Feed and the Low End Feed. The measured results show good agreement with the simulation of cascaded blocks which consists of the simulated two-port antenna and the measured 2-port S-parameters of the feeding network circuit. The latter consists of the baluns, coaxial cables and the power divider. Figure 40 shows the series and parallel resonance points calculated after de-embedding the effect of the baluns and cables as illustrated in Figure 41. As expected, according to the CM analysis discussed above (see Figure 26), the parallel resonance frequency point of the Low end Feed case occurs

before the corresponding resonance point for the Center Feed case.

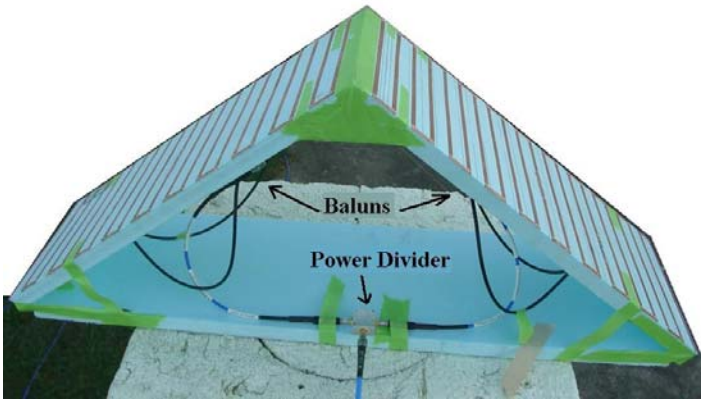

Figure 37 Vee-shaped meander line antenna feed with 2 baluns & 1 power divider

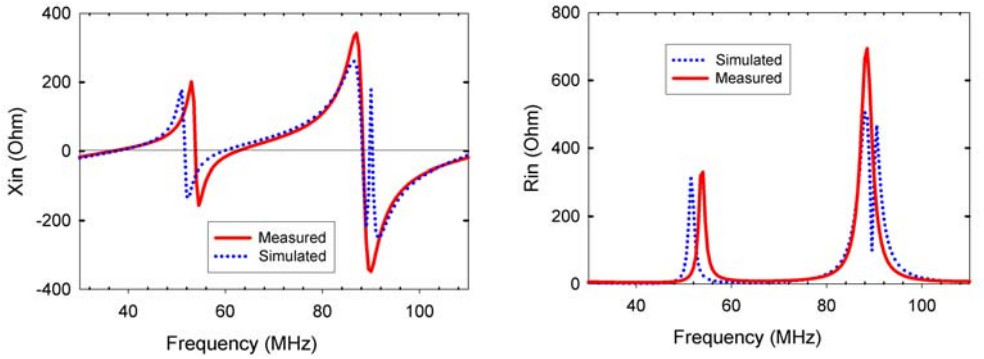

Figure 38 Measured Zin of the center fed antenna. Xin (Left) & Rin (Right)

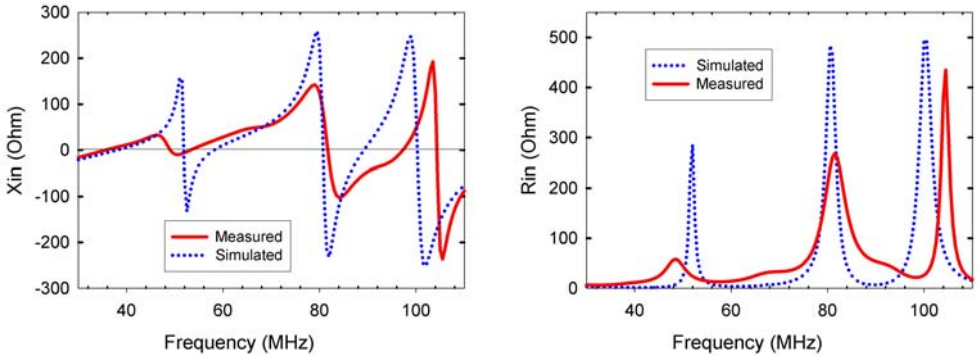

Figure 39 Measured Zin of the Low End feed antenna. Xin (Left) & Rin (Right)

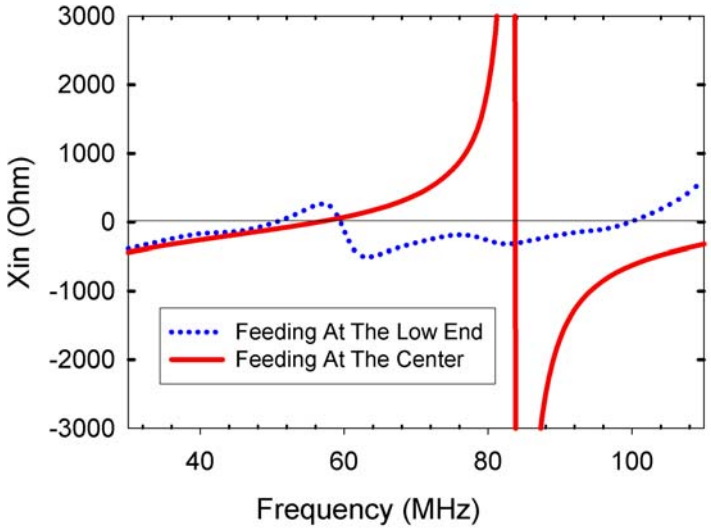

Figure 40 De-Embedded imaginary part of the Vee antenna. Center Feed vs. Low End Feed

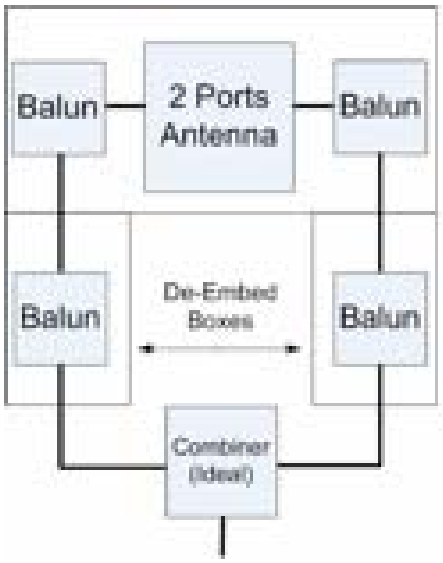

Figure 41 Block diagram of the measured 2 ports Manta and the two de-embedding boxes (balun + cables)

Figure 42 shows the measured gain of the center feed Vee antenna at both frequencies

ends (50 MHz and 100 MHz) which includes both the impedance mismatch and the loss in the baluns and power divider (loss is around -1dB). As expected from analysis and simulation results, as the frequency of operation increases, high order modes will affect the cross-pole gain level. To illustrate the effect of exciting the high order modes earlier as in the case of the low-end feed, the vertical polarization of the two feeding schemes are shown in Figure 43 at both 50 MHz and 100 MHz.

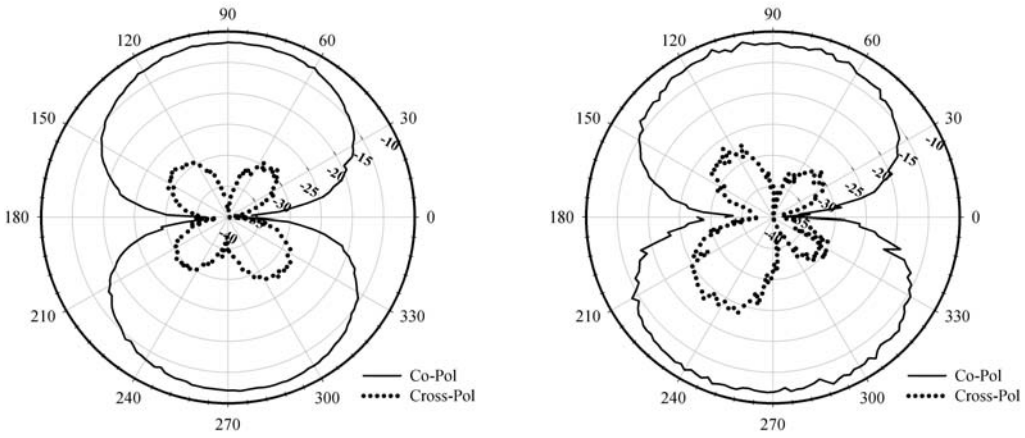

Figure 42 Measured gain in dB of the Center Feed antenna. 50 MHz (Left) & 100 MHz (Right)

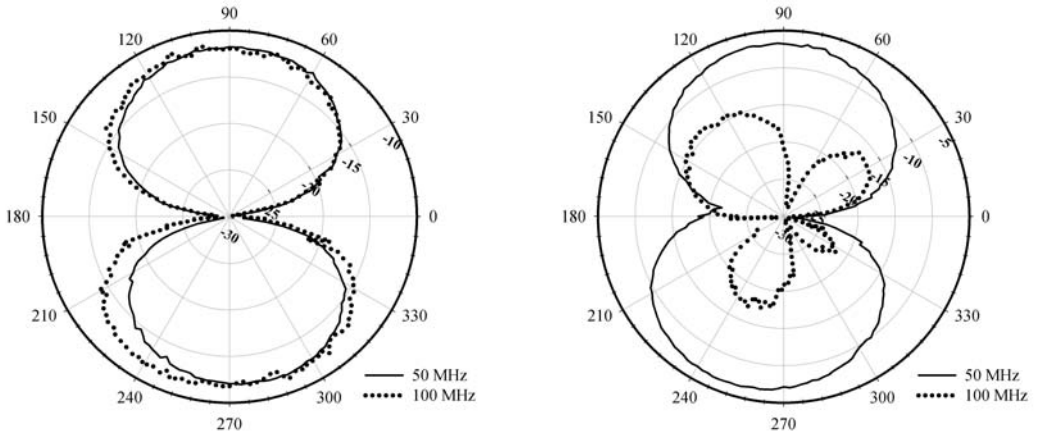

Figure 43 Measured gain in dB. Center Feed (Left) vs. Low End Feed (Right)

4.6 Conclusion

The theory of CM is used here to design and increase the bandwidth of an antenna conformal to the V-shaped tail of the Manta UAV. Simulated and measured results show that this method is accurate and very useful because it gives physical insight not generally available with other purely numerical techniques. The frequency bandwidth (pattern and input impedance) of this antenna can be increased even further with a more complex feeding network (4 ports or more) by suppressing the excitation of higher order modes. However, the complexity and losses in the feeding network will also increase. Thus, there is a trade off between bandwidth,complexity, efficiency and cost.

CHAPTER 5

DESIGN OF FREQUENCY RECONFIGURABLE ANTENNAS USING THE THEORY OF CHARACTERISTIC MODES

5.1Introduction

This chapter demonstrates a design procedure for frequency tunable reconfigurable antennas applying reactive loads [34]. Unlike other design procedures, antennas of arbitrary geometry can be tuned utilizing the proposed design framework. The design technique utilizes the theory of Network Characteristic Modes to systematically compute the load values required to resonate any antenna at many frequency points in a wide frequency range. For simplicity, a 1.2m dipole antenna is used to demonstrate the design procedure by tuning it at four loading ports along the antenna body. Both simulations and measurements demonstrate wide frequency tunability characteristics of the dipole input impedance (tunability range wider than 1:4) while preserving the radiation pattern and polarization at seven different frequency states.

Multifunction electrically small antennas have been gaining increasing attention in the last ten years due to the increased demand to cover with a single small antenna larger frequency bands and still maintain efficient behavior. As a result, a single reconfigurable antenna with narrow instantaneous bandwidth tunable over a wide frequency range can become part of the new generation of wireless products, especially with the recent

advances on Software Defined Radios (SDRs). Such design accompanying the reduction of either the non linearity of the PIN diodes or the complexity and cost of the MEMS switches which are needed to build tunable banks of capacitors or inductors, can alleviate the need for other analog filters in the RF front-end and provide wide bandwidth coverage with a single antenna.

This work proposes general design methodology applicable to electrically small to mid size antennas to effectively control the antenna current distribution at different frequency points over a wide frequency range using discrete reactive loading. Furthermore, this design methodology allows any type of full wave simulators to calculate the required loads for any type of antenna geometry. As a specific example, the proposed method will be applied to a linear wire dipole loaded with various discrete loads as shown in Figure 44. While discrete passive loading [35] Khaled Obeidat, Bryan D. Raines, and Roberto G. Rojas "Application of Characteristic Modes and Non-Foster Multiport Loading to the Design of Broadband Antennas" Volume 58, Issue 1, January 2010

[36] using the theory of Characteristic Modes have been used in the past to alter the Radar Cross Section (RCS) of a scatterer, its use to design reconfigurable frequency antenna is believed to be novel.

Figure 44 Loaded center-fed dipole antenna with four load circuits

Although several related works [44][45] were performed in the past to calculate the required passive reactance loads, their analytical framework depended on transmission line theory, which is not generally applicable when applied to electrically small and arbitrarily-shaped antennas. In other related work, [46] [47] calculation of the required loads rely on empirical parametric studies or computer optimization rather than a systematic design technique.

The proposed design methodology has the advantage of guaranteeing one dominant mode of operation at all the frequency points of interest even at frequencies where high order modes can be excited in the original unloaded antenna. In contrast, in previous work [45] the antenna geometry has been modified to eliminate the excitation of high order modes at high frequency.

5.2 Design Methodology

If the current distribution along the body of an antenna is controlled over wide frequency range using tunable loads at discrete frequency points (states), both the antenna input impedance and its radiation pattern are said to be widely tunable over that frequency range. The theory of Network Characteristic Modes (NCM) [35] Khaled Obeidat, Bryan D. Raines, and Roberto G. Rojas "Application of Characteristic Modes and Non-Foster Multiport Loading to the Design of Broadband Antennas" Volume 58, Issue 1, January 2010

[36] can systematically compute the load values which are required to force the

antenna to resonate different current shapes at different desired states. However, prior to calculating the load values, the locations of those loads along the antenna body should be carefully chosen. Furthermore, identifying the required current is very critical to obtain acceptable reflection coefficient S_{11} at the antenna feed, and to produce the desired radiation pattern at various states.

The theory of Network Characteristic Modes (NCM) for an antenna with N-port can be represented by an N-port *Z* matrix. The N eigenmodes are computed using the following generalized eigenvalue problem at some radial frequency ω [35] Khaled Obeidat, Bryan D. Raines, and Roberto G. Rojas "Application of Characteristic Modes and Non-Foster Multiport Loading to the Design of Broadband Antennas" Volume 58, Issue 1, January 2010

[36]:

$$\left[X_a(\omega)\right]\bar{I}_n(\omega) = \lambda_n(\omega)\left[R_a(\omega)\right]\bar{I}_n(\omega) \tag{5.1}$$

where $\left[R_a(\omega)\right]$ and $\left[X_a(\omega)\right]$ are, respectively, the real and the imaginary parts of the N-port $\left[Z_a(\omega)\right]$ open circuit impedance matrix of the antenna, $\bar{I}_n(\omega)$ is the n^{th} eigencurrent, and λ_n is the corresponding n^{th} eigenvalue.

The total current is therefore a weighted summation of all these modes [35] Khaled Obeidat, Bryan D. Raines, and Roberto G. Rojas "Application of Characteristic Modes and Non-Foster Multiport Loading to the Design of Broadband Antennas" Volume 58, Issue 1, January 2010

[36]:

$$\bar{I}(\omega) = -\sum_{n=1}^{N} \frac{\bar{I}^{*}\bar{V}_{oc}(\omega)}{1+j\lambda_n(\omega)}\,\bar{I}_n(\omega) = -\sum_{n=1}^{N}\alpha_n\,\bar{I}_n(\omega) \tag{5.2}$$

where $\bar{V}_{oc}(\omega)$ is the N-port open circuit voltage column vector of the N-port network characterized by $\left[Z_a(\omega)\right]$, and $(\cdot)^*$ indicates a Hermitian transpose. It is assumed that the modes are normalized such that $\bar{I}_n^*(\omega)\left[R_a(\omega)\right]\,\bar{I}_n(\omega)$ is equal to 1 (unit power).

Equation (5.2) has two important components to each modal current expansion coefficient. The denominator essentially depends on the frequency-dependent eigenvalue λ_n, which is a function solely of the antenna geometry and materials. The numerator is determined by an inner product between a frequency-dependent eigencurrent $\bar{I}_n(\omega)$ and the applied excitation $\bar{V}_{oc}(\omega)$.

The required lossless load reactance at the i^{th} port is given by [35] Khaled Obeidat, Bryan D. Raines, and Roberto G. Rojas "Application of Characteristic Modes and Non-Foster Multiport Loading to the Design of Broadband Antennas" Volume 58, Issue 1, January 2010

[36]:

$$X_{L_i}(\omega) = -\frac{1}{I_{d_i}(\omega)}\left(\left[X_a(\omega)\right]\bar{I}_d(\omega)\right)_i \tag{5.3}$$

where the subscript i denotes the i^{th} port and $\bar{I}_d$ is the desired equiphase current distribution. An eigencurrent $\bar{I}_n$ is in resonance when its corresponding eigenvalue λ_n

equals zero. The loads described by the diagonal matrix $\left[X_L(\omega)\right]$ are used to enforce the quantity $\left[X_a + X_L\right]\bar{I}_d$ to be zero. Consequently, the N-port current $\bar{I}_d$ is made the *dominant eigencurrent* at the desired frequency points.

5.3 Application: Frequency Reconfigurable Dipole Antenna

The proposed design technique is applicable to any antenna geometry; however, for simplicity, a planar copper dipole antenna of length 1.2 m and 6 mm width mounted on 3cm foam is considered here. For the purpose of measurements the dipole was connected to a ZFSCJ-2-1-S (Mini-Circuits) balun through two 0.33 m coaxial cables at each port of the balun. Seven different states were chosen to cover the frequency band down to 70 MHz (ka = 0.88, where a = 0.6m is the radius of the smallest circumscribing sphere about the dipole) and up to 300 MHz (ka = 1.2π), with a minimum operational tunable range of 4:1. The radiation pattern must substantially resemble the pattern shape of a λ/2 dipole. We have chosen to use the Method of Moments (MoM) codes ESP5.4 [24] and Momentum [48]. They will be used to extract the network Z parameters of the multiport dipole antenna, as well as input impedance and radiation pattern.

5.3.1 Port Setup

The first characteristic eigencurrent of the unloaded dipole [37] was chosen to resonate the dipole antenna at the desired states in order to produce the desired pattern shape at each state. The first eigencurrent of the unloaded dipole has its first resonance frequency at 115 MHz. Note that, for a center-fed dipole, Mode 2 does not contribute to

the total current because it is an odd mode [37].

Five ports were selected, with four loading ports symmetrically distributed along the dipole and one feeding port at the center of the antenna as illustrated in Figure 44. The locations of the load ports were chosen such that two ports are close to the center of the dipole where the current distribution is high in magnitude, and the remaining 2 ports are closer to the dipole ends. Given the port locations, the 5-port Z network parameters can be computed using(5.1).

5.3.2 Load Computation

The desired current distribution, which in this case corresponds to the first eigenmode of the 5-port network representation of the dipole at 115 MHz, is computed to be $\bar{I}_d = \left[0.66 \quad 0.98 \quad 1.0 \quad 0.98 \quad 0.66\right]^T$,*where* $[\cdot]^T$ indicates transpose. $\bar{I}_d$ was applied to equation (5.3) to extract the reactance values required to force the current $\bar{I}_d$ to be in resonance at seven frequencies distributed over 50 to 350 MHz as tabulated in Table 1. Reactance values for each state are shown in Figure 45 (seven heavy dots).

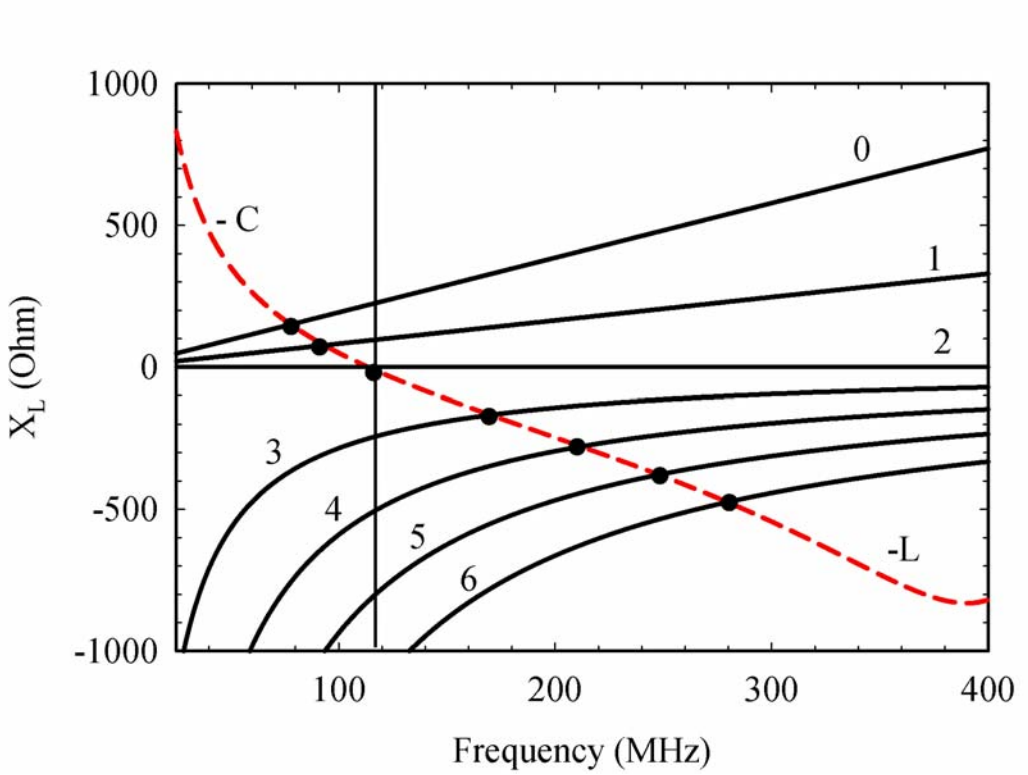

Figure 45 Required series reactances at port 2 of the seven states as specified in Table 1

Table 1 Load Element Values of the Loaded 4 Port Reconfigurable Dipole Antenna

State	Frequency (MHz)	Port 2	Port 1
0	70	307nH	491nH
1	90	131nH	170nH
2	115	shorted	shorted
3	180	5.6pF	4.7pF
4	225	2.7pF	2.2pF
5	270	1.7pF	1.3pF
6	300	1.2pF	1.0pF

Positive reactance values in Figure 45 were approximated by passive inductors at the corresponding frequency points, while negative reactance values were approximated by passive capacitors at the corresponding frequency points. Reactive element values for each state are tabulated in Table 1. State 2 represents the unloaded dipole antenna. States 0 and 1 represent the antenna with inductive loading, while States 3-6 represent the

antenna with capacitive loading. For this particular example, capacitive loading increases the resonant frequency, while inductive loading decreases the resonant frequency. This result is intuitive in that capacitive loading effectively shrinks the effective dipole length, while inductive loading extends the effective dipole length.

It is interesting to note that if we compute the reactances at each port as a function of frequency between 25 and 400 MHz and examine their frequency behavior, one can show that they have negative slopes (i.e. non-Foster). The reactance function for port 2 is shown as the dashed line in Figure 45. If such loads were realized exactly, the dipole antenna would be in continuous resonance at each single frequency between 25 and 400 MHz. For this example, the loads may be satisfactorily approximated by a series of LC circuit where both elements (L and C) have negative values (i.e. non-Foster elements), as shown in Table 2. This concept will be discussed in the next chapter. It is important to emphasize that the loads for the proposed reconfigurable antennas are passive Foster loads.

Table 2 Load Element Values Of The Loaded 4 Port Wide Band Dipole Antenna

Distance from center (cm)	0	±8.6	±34.3
L (nH)	-120.19	-207.87	-327.46
C (pF)	-14.78	-9.69	-4.97

5.3.3 Eigenvalue Analysis

Between 25 and 400 MHz, Modes 1 and 3 (the first two well-known even dipole modes) are dominant. The eigenvalue magnitudes (in decibels) of these two modes are

plotted for the capacitive and inductive loading cases in Figure 46 and Figure 47, respectively. From the eigenvalue spectrum of State 2, it may be observed that Mode 1 resonates at 115 MHz because its corresponding eigenvalue magnitude approaches zero (i.e. a resonant eigenmode at 115 MHz). Similarly, Mode 3 of State 2 resonates at 355 MHz. Similar conclusions can be drawn for the remaining states.

For the unloaded dipole, the modal resonance frequency of Mode 1 is the same as the impedance resonance frequency because the other modes are insignificant at this frequency (i.e. $|\alpha_1|$ is much larger than the other $|\alpha_k|$).

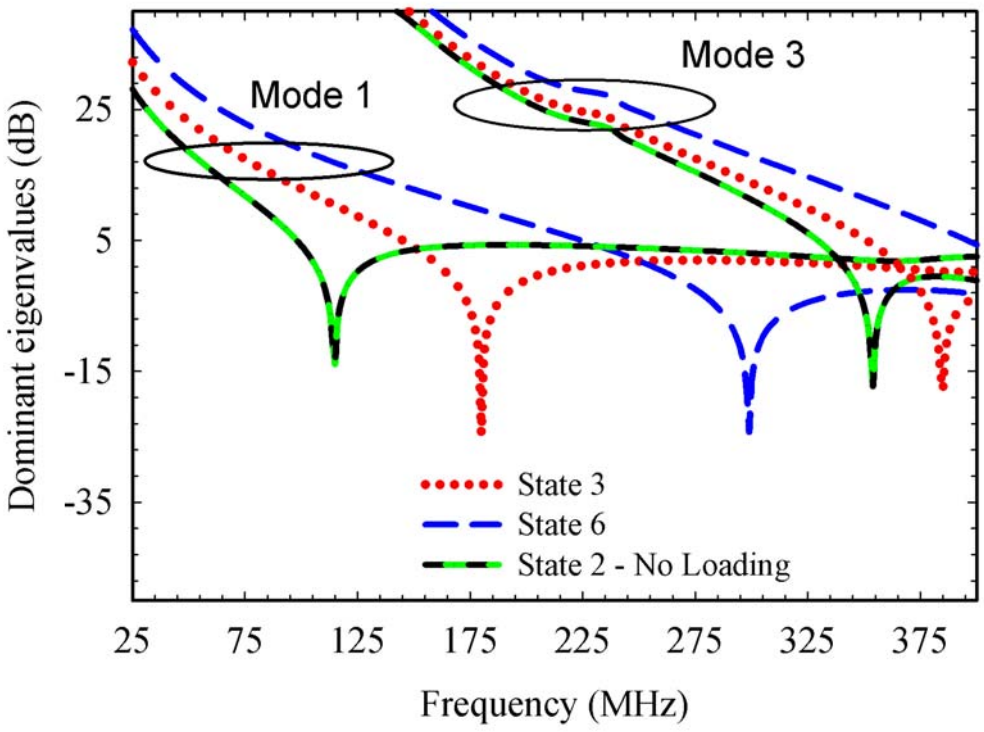

Figure 46 Eigenvalue spectrum of the 5-port 1.2 m dipole for both the unloaded case and for the capacitive loading case

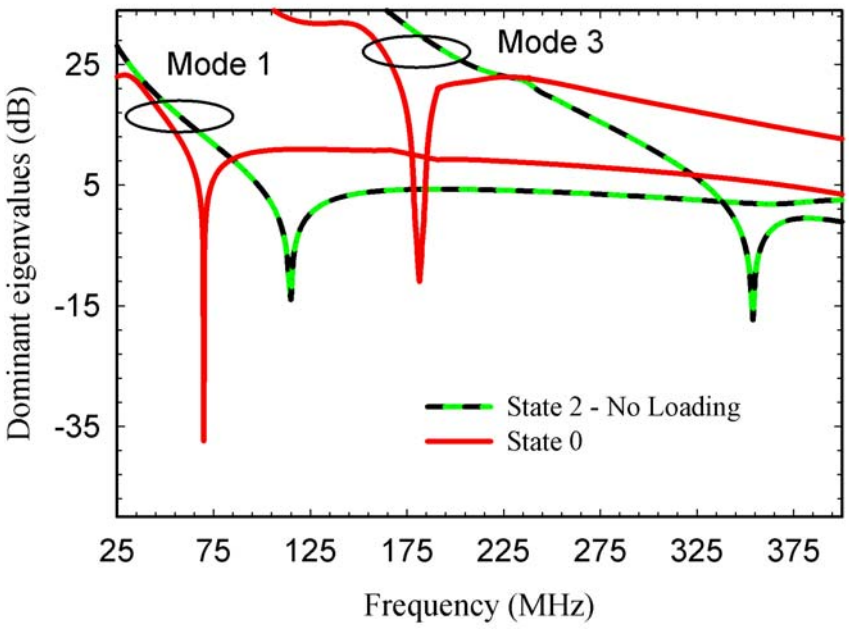

Figure 47 Eigenvalue spectrum of the 5-port 1.2 m dipole for both the unloaded case and for the inductive loading case

5.3.4 Current Analysis

To better understand the effect of the loads on the actual antenna current, the normalized magnitude of the antenna current distribution of the reconfigurable antenna was computed at 115, 180 and 300 MHz, respectively as shown in Figure 48. The desired current distribution is only specified at the 5 chosen port locations. In all of the curves, the actual current distribution closely follows the desired current distribution, except at 300 MHz (state 6), which demonstrates the greatly increased significance of Mode 3 at 300 MHz as the ratio $\left|\alpha_1 / \alpha_3\right|$ is decreasing. Clearly at 300 MHz the total current contains a noticeable contribution from higher order Mode 3 alongside the desired Mode 1.

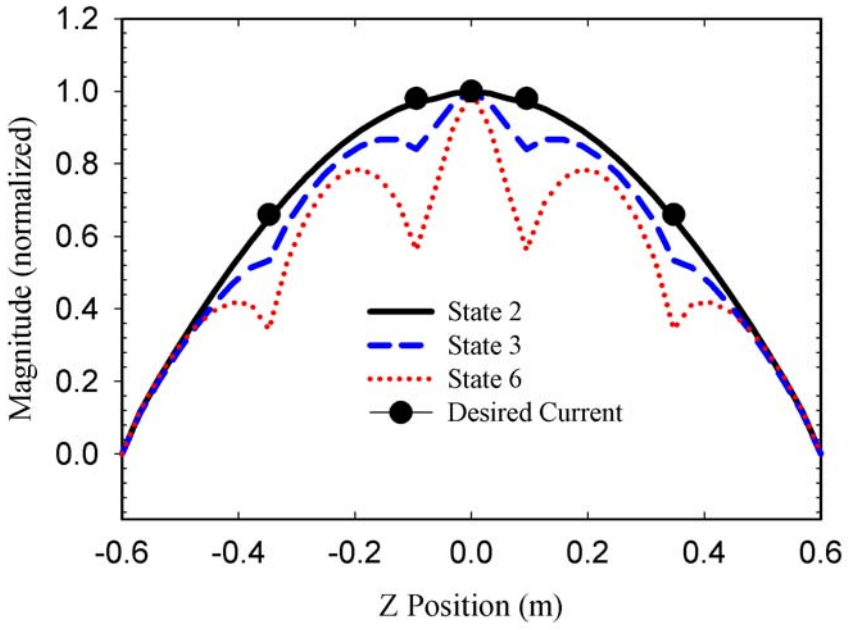

Figure 48 Comparison of the magnitude of the normalized desired current at five ports (dots) with the normalized antenna current distribution for the loading case reported by Momentum simulation at at 115 MHz, 180 MHz and 300 MHz

5.3.5 Input Impedance Analysis

The next key step in the design is to calculate an envelope of the S_{11} at the input feeding port of the antenna as shown in Figure 49 (dashed line). Each frequency point of the envelope is calculated by selecting the appropriate lossless reactive loads so the desired current is resonant at that frequency point. One example of a reactive load obtained to obtain the envelope is depicted by the dashed line in Figure 45 . The next step is to examine the envelope to determine the frequency range where the S_{11} magnitude is below a desired level.

For example, in Figure 49, if the desired S_{11} is below -10 dB, then the frequency range would be from 92-246 MHz. The chosen states fall within this frequency range, except for States 0, 1, 5, and 6. The performance of these four states will be improved using a passive matching network. Before discussing matching networks, this antenna was constructed and tested. The calculated reflection coefficient S_{11} of the reconfigurable antenna's input impedance seven states are shown in Figure 49 (solid lines) while the measured results are shown in Figure 50. The measured results were obtained by loading the antenna at its four ports a set of loads tabulated in Table 1. There is generally excellent agreement between the calculated and measured reflection coefficients for low frequency states, while more significant discrepancy between calculation and measurement is observed at high frequency states. This is mainly attributed to the fact that the 5-port Z network parameters used to derive the actual load inductor and capacitor values were calculated rather than measured. While the loaded dipole layout was carefully modeled, the parasitic effects are becoming more pronounced at the higher frequencies, especially with the lumped loads.

The proposed technique ensures nearly resistive input impedance for frequencies where high order eigenmodes are very weakly excited ($|\alpha_1 / \alpha_3| >> 1$). However, in the case of State 6, the value of $|\alpha_3|$ is comparable to $|\alpha_1|$. Therefore, Mode 3 will contribute more significantly to the total current and consequently, the total current $\bar{I}$, as determined by equation (5.2), will not satisfy $\left[X_a + X_L\right] \bar{I} = 0$ at high frequencies. This quality implies a non-zero reactance at the feed port at high frequencies ($\sim > 250$ MHz) and

consequently a lower reflection coefficient. More control of Mode 3 can be achieved if additional ports are introduced; however, there has to be tradeoff between number of ports/complexity and larger bandwidth. On the other hand, at low frequencies of operation, namely States 0 and 1, the antenna electrical size is small with small radiation resistances; therefore, larger reflection coefficients are expected.

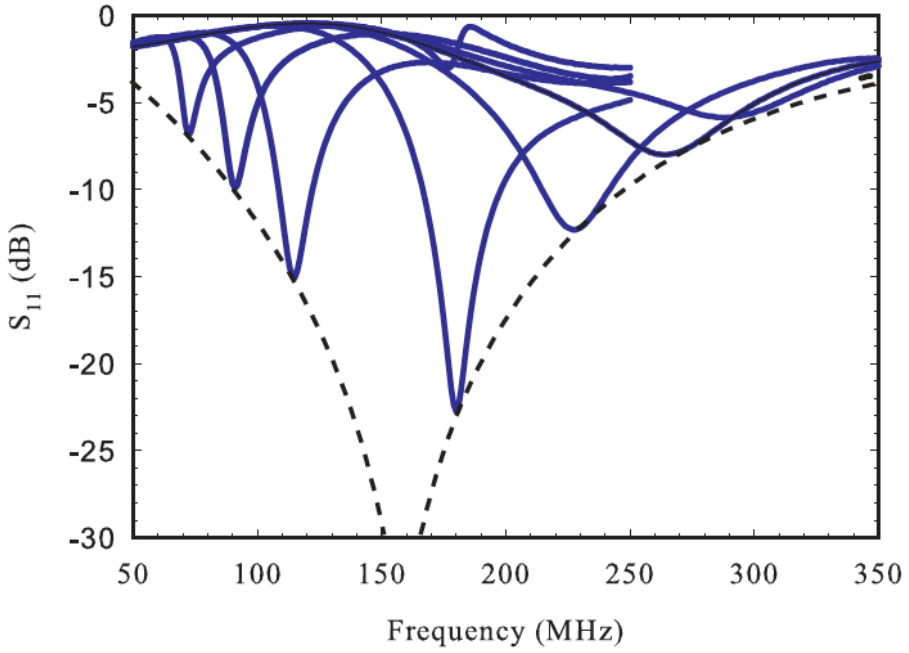

Figure 49 The calculated return loss S_{11} of the dipole antenna for the *non – Foster loading* case (Dashed) and for the *passive loading* cases (Solid) all referenced to 50 Ω

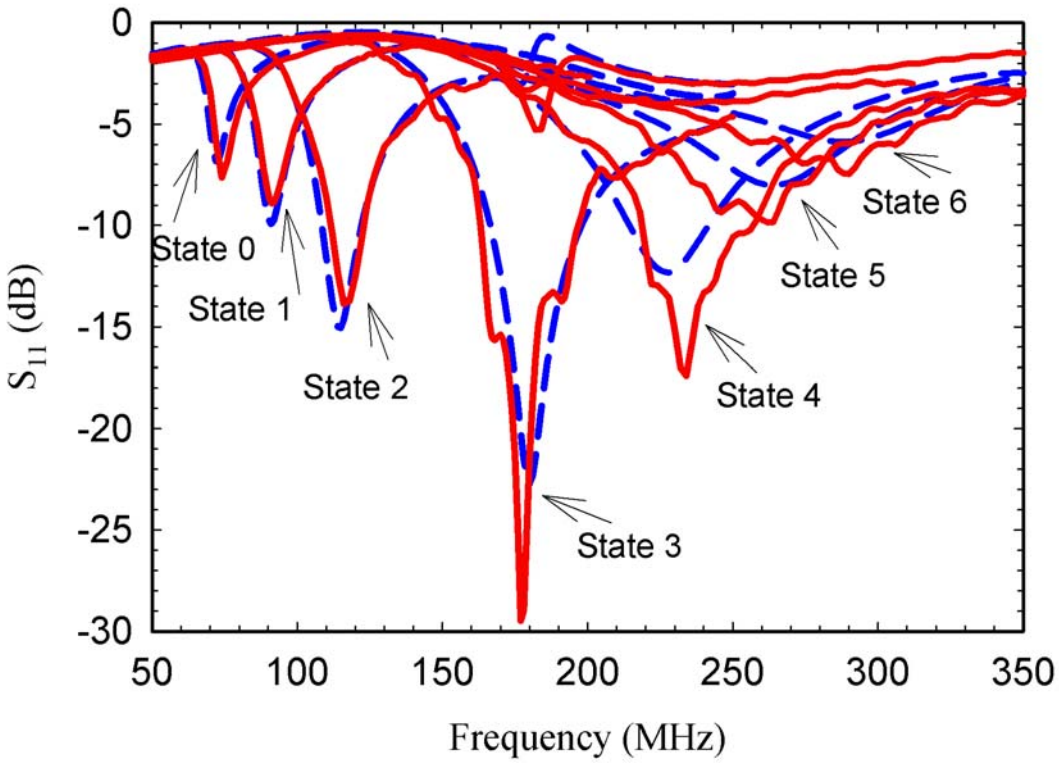

Figure 50 The return loss S_{11} of the reconfigurable dipole antenna, Simulated (Dashed) vs. Measured (Solid)

Another important advantage of the envelope is in the design of the matching network to enhance the performance of the seven states all at once. A single passive matching network can be designed by considering the envelope as the load. Figure 51 shows the reflection coefficient S_{11} of the cascaded combination of the measured antenna S_{11} and the two-port simulated matching network S-parameters. The matching network is a lossless seventh-order passive ladder matching circuit designed from 65-300 MHz using the Real Frequency Technique [7].

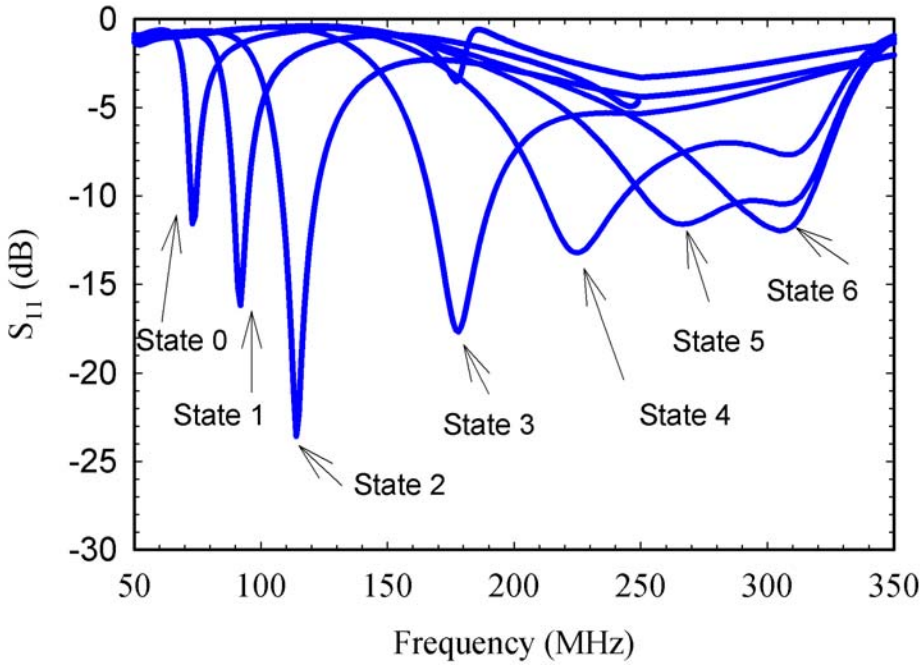

Figure 51 The return loss S_{11} of the reconfigurable dipole antenna with ideal lossless matching network

5.3.6 Radiation Pattern Analysis

The radiation pattern at the desired tunable frequency points (States) is also important. Figure 52 illustrates the measured realized gain of the loaded antenna at 74 MHz (State 0) and the unloaded antenna at 114 MHz (State 2), Figure 53 illustrates the measured realized gain of the loaded antenna at 290 MHz (State 6) and the unloaded antenna at 114 MHz (State 2), and Figure 54 illustrates the measured realized gain of the loaded antenna at 290 MHz (State 6) and the unloaded antenna at the same frequency point. As far as the pattern is concerned, it is obvious that loading the antenna has

extended the desired pattern shape seen at 70 MHz up to 300 MHz by suppressing higher-order modes. The pattern at 300 MHz still resembles the desired pattern shape, even though the total current has some contribution from Mode 3 because a first-order error in current manifests itself as a second-order error in the far-field.

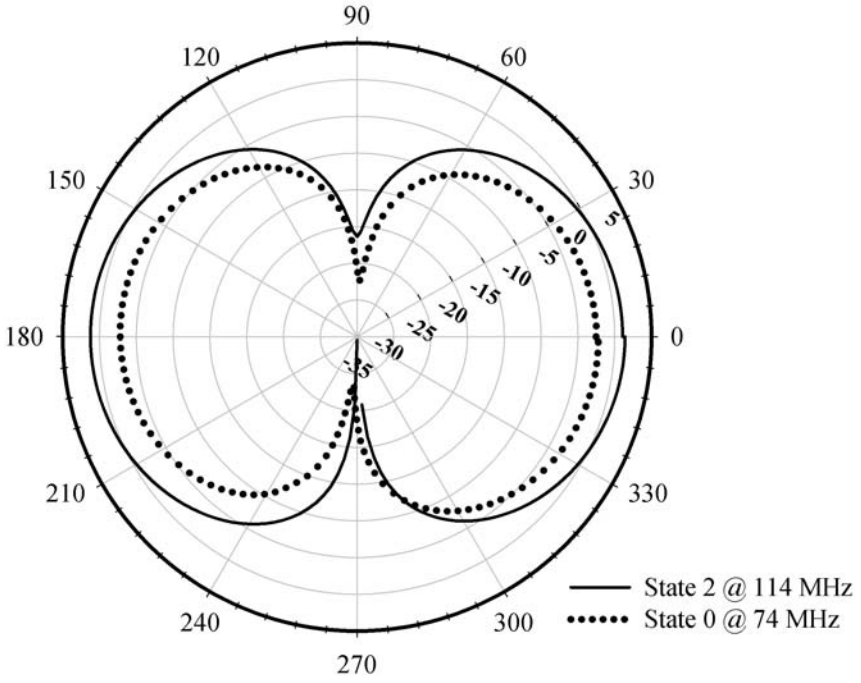

Figure 52 The measured realized gain in dB of the loaded dipole antenna (State 0) at 74MHz compared to the unloaded dipole antenna (State 2) at 114MHz

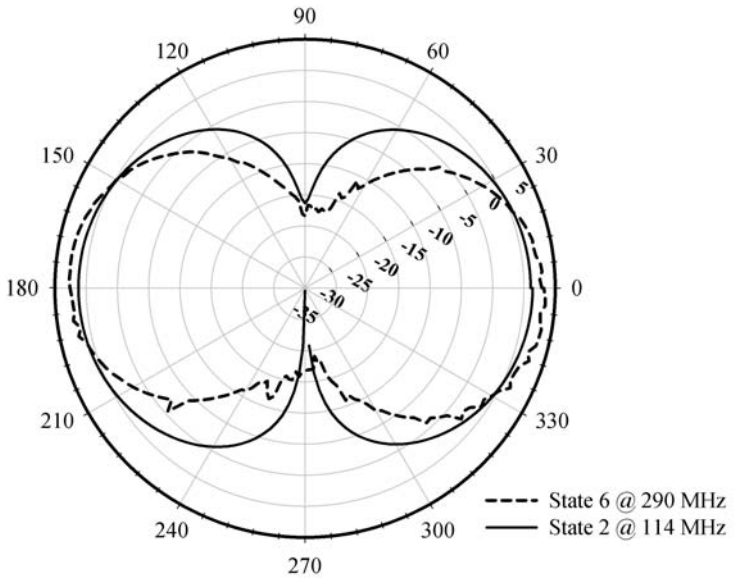

Figure 53 The measured realized gain in dB of the loaded dipole antenna (State 6) at 290MHz compared to the unloaded dipole antenna (State 2) at 114MHz

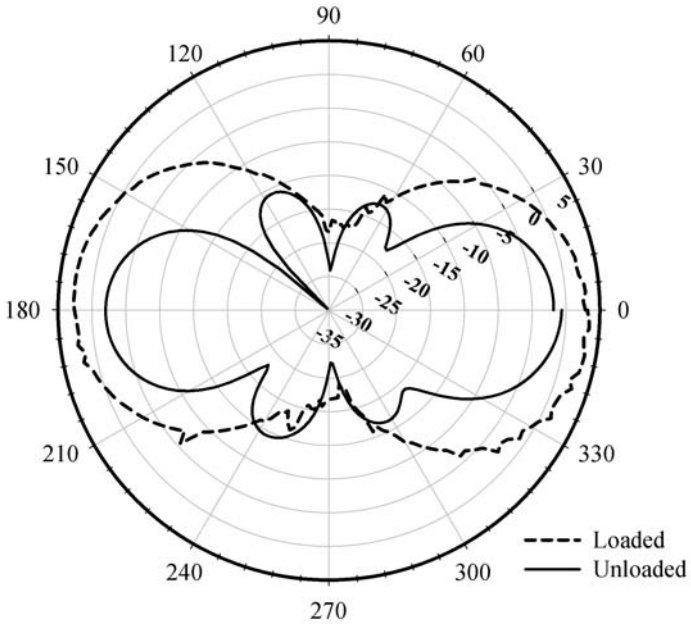

Figure 54 The measured realized gain in dB of the loaded dipole antenna (State 6) compared to the unloaded case at 290MHz

5.4 Conclusion

In this chapter, the theory of Network Characteristic Modes (NCM) was proposed to systematically design widely tunable reconfigurable antennas of arbitrary shape. As an example, the method was applied successfully to a simple 1.2m dipole antenna from 70 MHz to 300 MHz. The dipole antenna was loaded with a set of different reactive elements at each state. Both pattern and input impedance of the loaded dipole antenna were successfully controlled at the tunable frequency points over wide frequency range.

A key concept introduced here to facilitate the design of the reconfigurable antennas is the calculation of the S_{11} envelope. The S_{11} envelope was computed and used for two different purposes. It was used to determine the minimum frequency range of states which yield acceptable S_{11} levels. Also, the envelope was used as the load to design a single passive matching network which would improve the input reflection coefficient levels of all states.

Finally, it should be observed that although the example presented in this chapter was used to design frequency tunable reconfigurable antennas, it can also be used to design pattern tunable antennas or a mix of pattern and frequency tunable antennas.

CHAPTER 6

APPLICATION OF CHARACTERISTIC MODES AND NON-FOSTER MULTIPORT LOADING TO THE DESIGN OF BROADBAND ANTENNAS

6.1 Introduction

A conceptual framework is proposed to systematically design antennas with broadband impedance and pattern characteristics using multiple reactive loads [35]. Antennas of arbitrary geometry can have their bandwidths expanded using this technique. The technique is applied to a narrow band thin wire dipole antenna to demonstrate its main features. It is shown that the loaded antenna resonates a desired current over a wide frequency band. The loads are shown to require non-Foster elements when realized. Simulations demonstrate the broadband characteristics of both the dipole input impedance and radiation pattern.

Wideband antennas have been the subject of extensive research, especially over the past ten years. The goal has been to obtain an antenna design with relatively constant pattern and impedance over some desired broad frequency range. Furthermore, market pressures for miniaturizing communication devices have encouraged the use of electrically small antennas and highly integrated RF circuitry. Electrically small antennas, however, have been shown to be fundamentally limited in bandwidth by the Chu limit

[1]. Traditionally, matching networks have been used at the feed points of such antennas to improve their impedance bandwidth; however, matching networks do not directly address the problem of a potentially changing radiation pattern at higher frequencies, where the antenna features become electrically large. On the other hand, the theories of frequency-independent antennas [27] and ultra-wideband antennas [28], can yield wideband antennas, but only directly apply to electrically large antennas.

In general, the best realizable electrically small antenna should only require a minimally complex matching network and should maintain a particular radiation pattern over a wide frequency range. Both of these aspects are essentially dependent on the antenna current. Wideband behavior may therefore be obtained by carefully shaping the antenna current distribution over frequency through changes to the antenna geometry, loading, or material composition.

This work proposes a general design methodology which effectively controls the antenna current distribution over frequency using discrete loading. As a specific example, the proposed method will be applied to a linear wire dipole loaded with various discrete loads. It will be shown that for the best wideband control, non-Foster loads are required. While discrete non-Foster loading [29], [30], [31] and characteristic mode theory [32], [33] have been separately used in the past to extend the operational bandwidth of antennas, their combination is believed to be novel.

As a point of comparison, a related work [27], [29] was performed in the past by loading a dipole with negative inductors instead of negative resonators. It differs from the proposed technique in that arbitrary control over the current distribution shape was not

achieved in [27], [29] because such loading can only have one unique mode of operation. Unlike the proposed scheme, this previous work is only applicable to a small subset of antenna current distributions and geometries. Therefore, although this previous work established wideband operation of a loaded dipole antenna for both input impedance and pattern metrics, it did not actually provide a general scheme for the control of an arbitrary current distribution (and therefore, pattern) on arbitrary antenna geometry. Furthermore, unlike the proposed technique, the analytical framework of the past work depended on transmission line theory, which is not generally applicable when applied to electrically small and arbitrarily-shaped antennas.

6.2 Design Methodology

If the current distribution over the body of an antenna can be controlled over a wide frequency bandwidth, the antenna input impedance and the radiation pattern can also be controlled. In this chapter, the control of the current distribution over some bandwidth through careful placement of multiple lumped will be explored, discrete loads. The theory of Network Characteristic Modes (NCM) [35] Khaled Obeidat, Bryan D. Raines, and Roberto G. Rojas "Application of Characteristic Modes and Non-Foster Multiport Loading to the Design of Broadband Antennas" Volume 58, Issue 1, January 2010

[36] is utilized in this chapter to design these loads which, together with the antenna, resonate a desired current distribution over the antenna body.

There are three important decisions related to the design of a wideband antenna through current distribution control using multiple discrete loads. First, a desirable

current distribution over the entire frequency band must be identified according to some metric. Second, the number and location of the loads should be determined. Third, the loads must be computed and subsequently realized over the desired frequency band. The design process will be aided through insights derived from (network) characteristic mode theory. The process is summarized graphically in Figure 55.

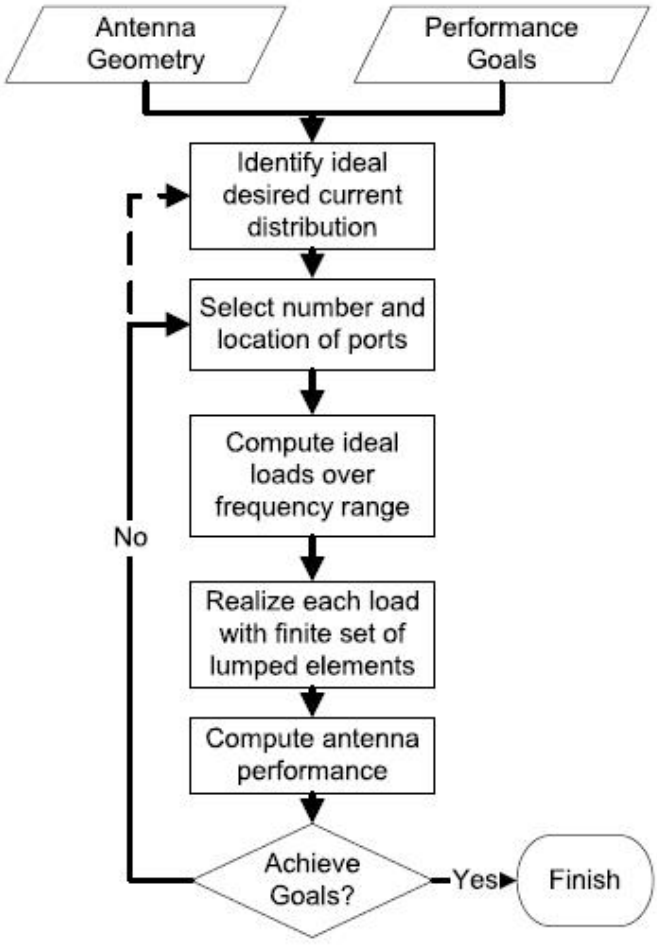

Figure 55 Flowchart of the design methodology

Identifying the required current is very critical to obtain a current with small magnitude variation versus frequency variation at the antenna feed (low impedance Q

factor) which should facilitate the design of a wideband passive matching network, and to produce the desired radiation pattern over the desired frequency band.

Before discussing load computation, a brief background on the theory of Network Characteristic Modes is provided. Although the theory of characteristic modes has historically been applied to the Method of Moments (MoM) impedance matrix, it is also possible to apply it to N-port Z networks, as in [35] Khaled Obeidat, Bryan D. Raines, and Roberto G. Rojas "Application of Characteristic Modes and Non-Foster Multiport Loading to the Design of Broadband Antennas" Volume 58, Issue 1, January 2010

[36]. This choice allows any suitable computational electromagnetic code or experimental method to determine the N-port network matrix.

The theory of Network Characteristic Modes (NCM) for an antenna with N-port can be represented by an N-port Z matrix. The N eigenmodes are computed using the following generalized eigenvalue problem at some radial frequency ω [35] Khaled Obeidat, Bryan D. Raines, and Roberto G. Rojas "Application of Characteristic Modes and Non-Foster Multiport Loading to the Design of Broadband Antennas" Volume 58, Issue 1, January 2010

[36]:

$$\left[X_a(\omega)\right]\bar{I}_n(\omega) = \lambda_n(\omega)\left[R_a(\omega)\right]\bar{I}_n(\omega) \tag{6.1}$$

where $\left[R_a(\omega)\right]$ and $\left[X_a(\omega)\right]$ are, respectively, the real and the imaginary parts of the N-port $\left[Z_a(\omega)\right]$ open circuit impedance matrix of the antenna, $\bar{I}_n(\omega)$ is the n^{th}

eigencurrent, and λ_n is the corresponding n^{th} eigenmode.

The total current is therefore a weighted summation of all these modes [35] Khaled Obeidat, Bryan D. Raines, and Roberto G. Rojas "Application of Characteristic Modes and Non-Foster Multiport Loading to the Design of Broadband Antennas" Volume 58, Issue 1, January 2010

[36]:

$$\bar{I}(\omega) = -\sum_{n=1}^{N} \frac{\bar{I}^{*}\bar{V}_{oc}(\omega)}{1+j\lambda_n(\omega)} \bar{I}_n(\omega), \tag{6.2}$$

where $\bar{V}_{oc}(\omega)$ is the N-port open circuit voltage column vector of the N-port network characterized by $\left[Z_a(\omega)\right]$, and $(\cdot)^*$ indicates a Hermitian transpose. It is assumed that the modes are normalized such that $\bar{I}_n^*(\omega)\left[R_a(\omega)\right]\bar{I}_n(\omega)$ is equal to 1.

Equation (6.2) has two important components to each modal current expansion coefficient. The denominator essentially depends on the frequency-dependent eigenvalue λ_n, which is a function solely of the antenna geometry and materials. The numerator is determined by an inner product between a frequency-dependent eigencurrent $\bar{I}_n(\omega)$ and the applied excitation $\bar{V}_{oc}(\omega)$.

The required lossless load reactance at the i^{th} port is given by [35] Khaled Obeidat, Bryan D. Raines, and Roberto G. Rojas "Application of Characteristic Modes and Non-Foster Multiport Loading to the Design of Broadband Antennas" Volume 58, Issue 1, January 2010

[36]:

$$X_{L_i}(\omega) = -\frac{1}{I_{d_i}(\omega)}\Big(\big[X_a(\omega)\big]\bar{I}_d(\omega)\Big)_i \tag{6.3}$$

where the subscript i denotes the i^{th} port and $\bar{I}_d$ is the desired equiphase current distribution. An eigencurrent $\bar{I}_n$ is in resonance when its corresponding eigenvalue λ_n equals zero. The loads described by the diagonal matrix $\big[X_L(\omega)\big]$ are used to enforce the quantity $\big[X_a + X_L\big]\bar{I}_d$ to be zero. Consequently, the N-port current $\bar{I}_d$ is made the *dominant eigencurrent* at the desired frequency points.

After the frequency variation of each reactive load is computed over the frequency range of interest, each load is approximated using a finite number of lumped reactive circuit elements. For the purposes of this chapter, we shall allow the elements to be both Foster and non-Foster (elements with negative frequency derivatives) in nature. For the example provided, it will be shown that the computed loads are non-Foster in nature over a wide frequency band. Non-Foster elements may be approximately realized using negative impedance converters [20], [21], [22].

6.3 Example

The proposed design technique is applicable to any antenna; however, for simplicity, a thin wire copper dipole antenna of length 1.2 m and 1 mm radius is considered here. This antenna is known to be a narrowband resonant antenna. However,

using the loading scheme proposed here, it can become a wideband antenna. The goal is to operate down to at least 50 MHz ($ka = 0.628$, where $a = 0.6m$ is the radius of the smallest circumscribing sphere about the dipole) and up to as high of a frequency as possible, with a minimum operational bandwidth of 4:1. The radiation pattern must substantially resemble a TM_{01} mode.

The Method of Moments (MoM) code ESP5.4 [24] was used to extract the network Z parameters of the multiport dipole antenna, as well as input impedance and radiation pattern. ESP5 automatically generates frequency-dependent wire segmentation in order to yield reliable results over the desired frequency band.

6.3.1 Identification of Desired Dipole Current Distribution

Since the goal is to obtain a wideband radiation pattern that resembles the TM_{01} spherical mode, the desired current distribution is the first eigenmode of the unloaded dipole [37]. Furthermore, if the first eigenmode is selected to resonate over the entire desired frequency band, it produces the desired pattern shape over that band. Thus, the desired current distribution is selected to be the first eigenmode at the lowest operational frequency, i.e. 50 MHz. The actual computation of the mode using equation (6.1) will necessarily have to wait until after the ports are selected.

6.3.2 Dipole Port Placement

Since this eigenmode will be computed using network characteristic mode theory,

we must first define the number and locations of the load points. Five ports were selected, with four ports symmetrically distributed along the dipole and one port at the middle of the antenna, which shall also serve as the feed point. The locations of the load ports (see Figure 56 were chosen such that the majority of ports are in regions where the current distribution is high in magnitude -- that is, close to the dipole center -- and the remaining 2 ports are closer to the dipole ends. Before the loads are determined, it is instructive to calculate the eigenvalue spectrum of the 5-port unloaded dipole. The spectrum is depicted in Figure 57 and, as expected, the dominant eigenvalue (λ_1) resonates at $f = 120$ MHz. The desired current distribution is computed to be $\bar{I}_d = \left[0.68 \quad 0.98 \quad 1.0 \; 0.98 \quad 0.68\right]^T$, where $[\cdot]^T$ indicates transpose.

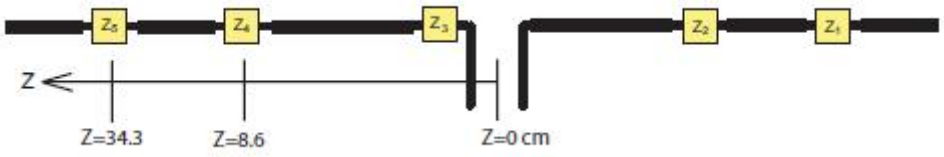

Figure 56 Loaded center-fed dipole antenna with multiple load circuits. Port 1 is on the extreme right, and the port numbers increase going to the left.

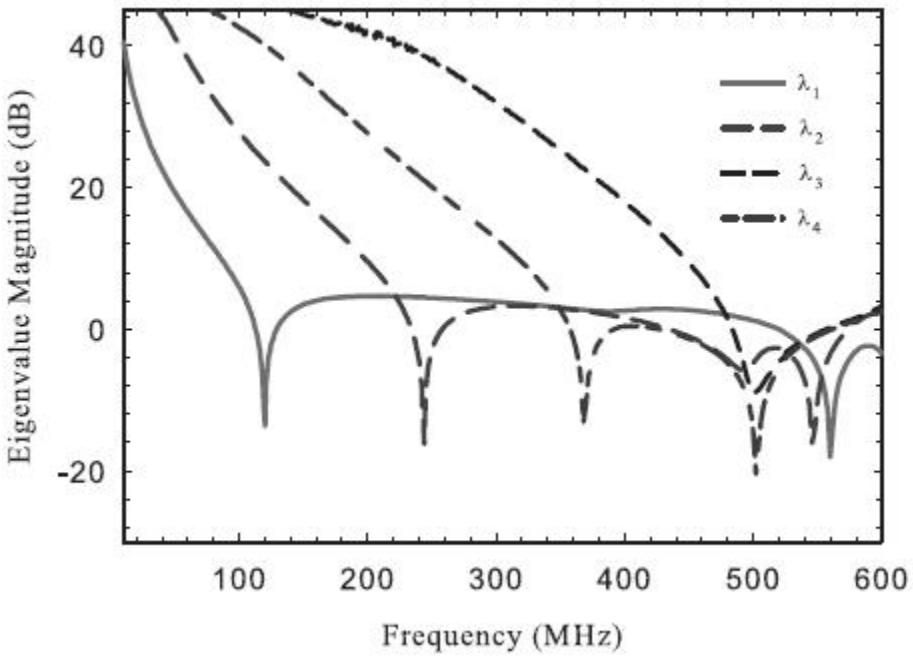

Figure 57 Eigenvalue spectrum of 5-port unloaded 1.2 m dipole

6.3.3 Dipole Load Computation

Given the desired current distribution and the set of 5-port Z parameters over the frequency band of interest, it is now straightforward to compute the reactance of each load versus frequency using equation(6.3). The results for this example have been computed for three cases: perfect loading, approximate loading, and no loading.

In the *perfect loading* case, the exact reactances computed in equation (6.3) are used, implying an infinitely complex reactive network is used at each load port to "realize" the reactance frequency behavior at that port. Two of the exact reactance curves are plotted versus frequency in Figure 58.

In the *approximate loading* case, the exact reactance computed from equation (6.3) at each port is approximated by a *finite number of lumped* reactive elements. After examining the frequency behavior of the exact computed reactances, it was found that the reactance at each port may be satisfactorily approximated by a series LC circuit where both elements (L and C) have negative values (i.e. non-Foster elements), as shown in Table 3. Lastly, the *unloaded* case describes the dipole antenna without loads.

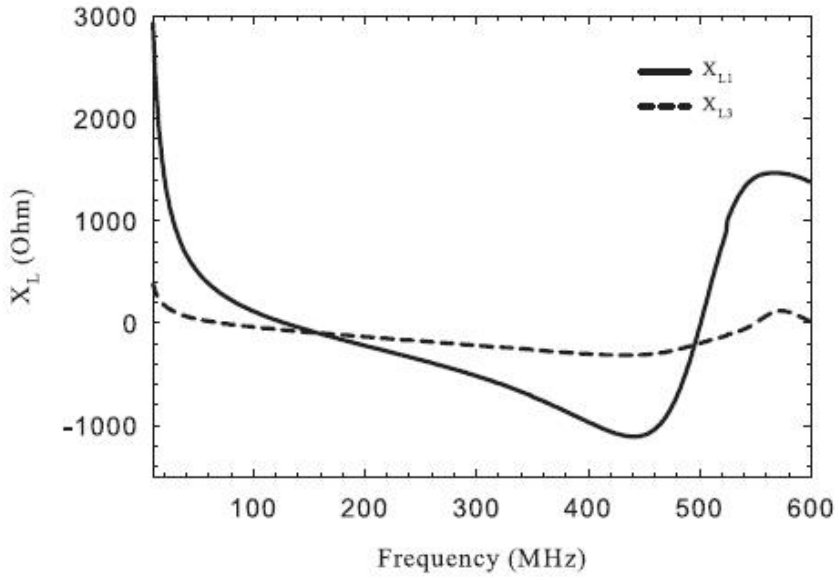

Figure 58 Required series reactances (as specified by $[X_L]$) at ports 1 (near the end of the dipole) and 3 (at the dipole center)

Table 3 Load element values of the loaded 5 port dipole antenna

Distance from center (cm)	0	±8.6	±34.3
L (nH)	-120.19	-207.87	-327.46
C (pF)	-14.78	-9.69	-4.97

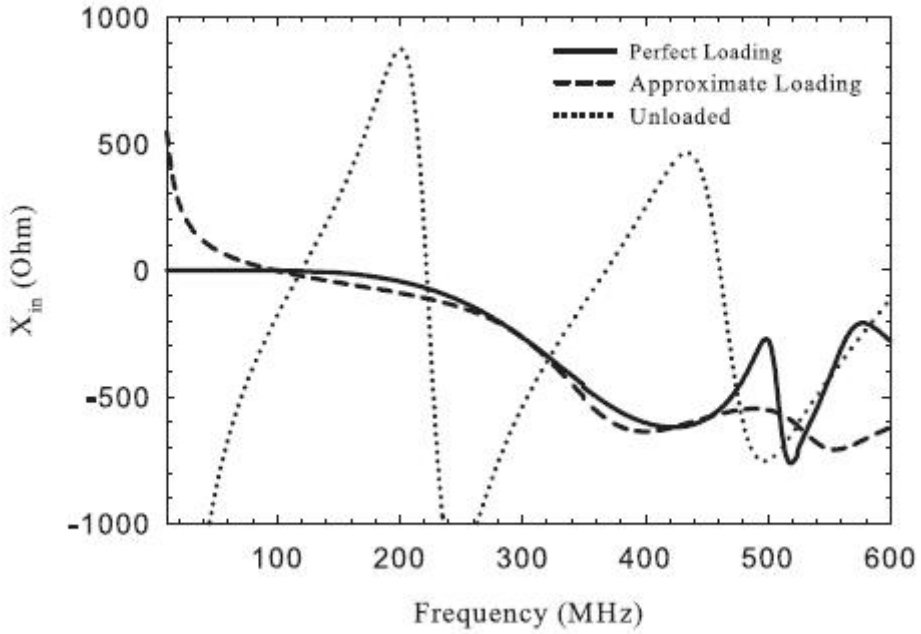

Figure 59 Input reactance X_{in} at the feed port of the dipole antenna for the *perfect loading* , *approximate loading* , and *unloaded* cases

6.3.4 Impedance Analysis

The value of the input reactance at the feed port (X_{in}) with and without loading is shown in Figure 59. It is apparent from Figure 59 that the magnitude of the reactance of the loaded dipole is smaller than the unloaded dipole, as well as more slowly varying in frequency. This behavior implies that it is easier to match the loaded dipole as compared to the unloaded dipole. The proposed technique ensures a nearly resistive feed point input impedance for frequencies where higher order eigenmodes are very weakly excited ($|\lambda_i| >> |\lambda_d|, i \neq d$), as shown in Figure 60. However, as the frequency becomes higher, the electrical size of the antenna increases, which tends to excite higher order modes

alongside the desired mode (where $\lambda_d = 0$).

Consequently, for a fixed number and position of the ports, the total current $\bar{I}$, as determined by (6.2), will not satisfy $\left[X_a + X_L\right]\bar{I} = 0$ at high frequencies, even in the *perfect loading* case. This implies a larger reactance at the feed port at high frequencies ($\sim> 250$ MHz). As expected, the *perfect loaded* case generally yields the best possible frequency bandwidth performance. For the *approximate loading* case, the reactance at the feed port is small, but non-zero, for most frequencies between 50 MHz and 200 MHz. In this example, ideal loads have a high slope (e.g., see load 1 in Figure 58) below 50 MHz and it is difficult to accurately match this behavior with the approximate loads. Consequently, the input reactance for the approximate loading case is higher (below 50 MHz) than the perfect loading case (see Figure 59). To further increase the bandwidth of the antenna, additional posts are needed to better control the current.

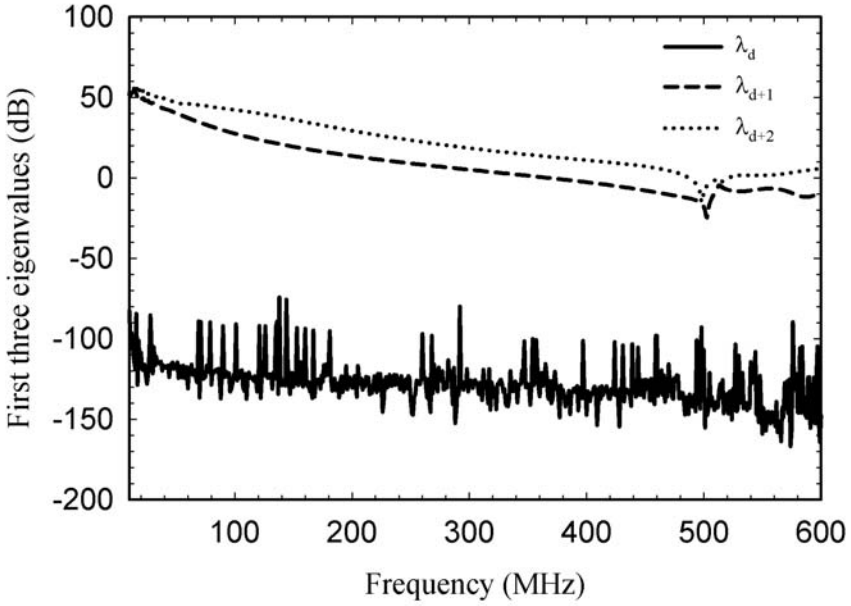

Figure 60 Values (in dB) of the first three dominant eigenvalues of the 5-port dipole antenna matrix for the perfect loading case. Note that, λ_{d+1} corresponds to an odd mode which will not contribute to the total current of a center-fed dipole

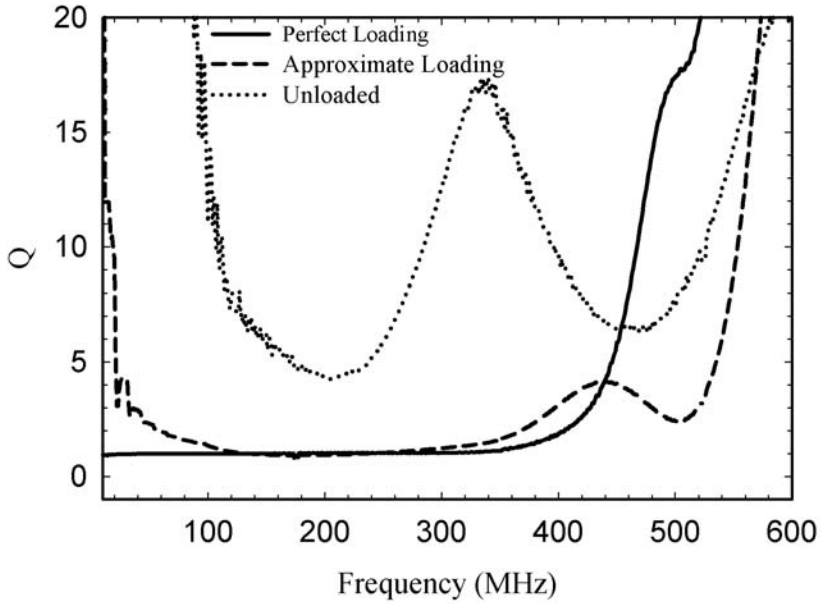

Figure 61 he Q factor of the dipole antenna for the perfect loading, approximate loading, and unloaded cases

The calculated Q using equation (96) in [17] is shown in Figure 61. It is evident that the loaded antenna Q is significantly reduced compared to the *unloaded* case up to 400 MHz, implying that the loaded antenna bandwidth has a greater potential for expansion. To further clarify the improvement in antenna Q, especially when the dipole is electrically small, it is useful to compare these results against the Chu limit. At 20 MHz, the circumscribing sphere electrical size is $ka = 0.25$. The Chu limit is approximately 67, the *unloaded* case has a Q of 1899, the *approximate loading* case has a Q of about 7, and the *perfect loading* case has a Q of only 1.

The loaded antenna return loss referenced to $50\,\Omega$ is shown in Figure 62. The improvement in the input impedance bandwidth using multiple loads is clear. For an S_{11} *level of* -7 dB, the *unloaded* antenna impedance bandwidth is 1.11:1 (114-126 MHz), while the *approximate loading* case yields a bandwidth of 2.59:1 (61-158 MHz). The antenna bandwidth may of course be enhanced further by using a passive matching circuit placed at the feed port (see insert in Figure 62). The improved input impedance of 7.64:1 (47-359 MHz) is shown in Figure 62 when a lossless seventh-order passive lumped element ladder matching circuit (designed using the Real Frequency Technique [7] from 10-350 MHz) is used at the feed port of the dipole with *approximate loading*. Note that $ka = 0.59$ at 47 MHz for the 1.2 m long dipole.

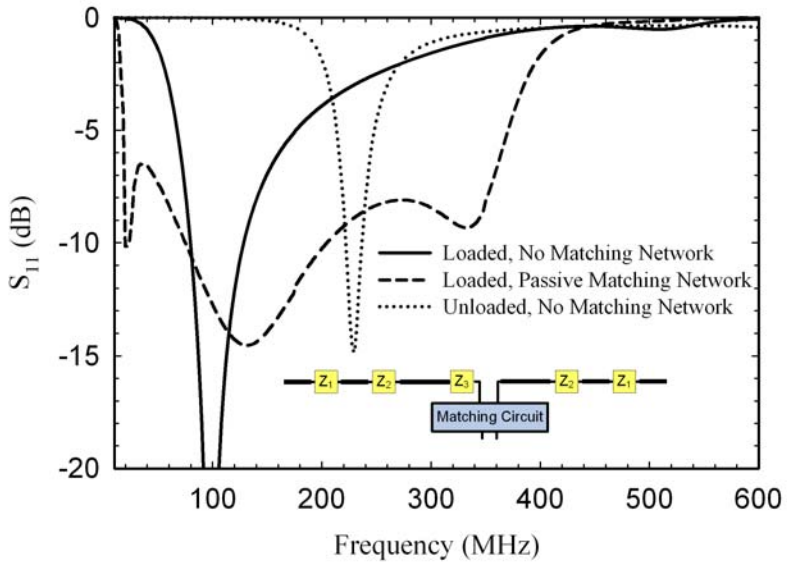

Figure 62 The return loss S_{11} of the unloaded dipole verses approximately loaded dipole antenna with and without the passive lumped element matching circuit (seventh order), all referenced to 50 Ω

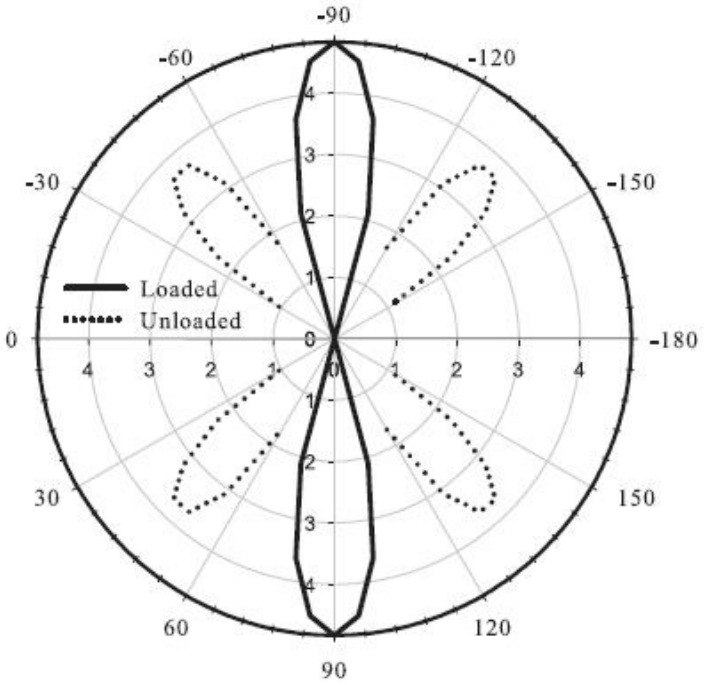

Figure 63 The gain in dB at 400MHz of the approximately loaded dipole antenna compared to the unloaded antenna (excluding input impedance mismatch losses)

6.3.5 Radiation Pattern Analysis

When discussing bandwidth, it is usually insufficient to solely consider antenna input impedance bandwidth, since the radiation pattern over the desired frequency band is also important. Figure 63 illustrate the gain of the unloaded and approximately loaded antenna at 400 MHz, respectively. As far as the pattern is concerned, loading the antenna can extend the desired pattern shape up to 400 MHz by suppressing higher-order modes. Between 400 and 500 MHz, the antenna pattern degrades into the third dipole mode pattern.

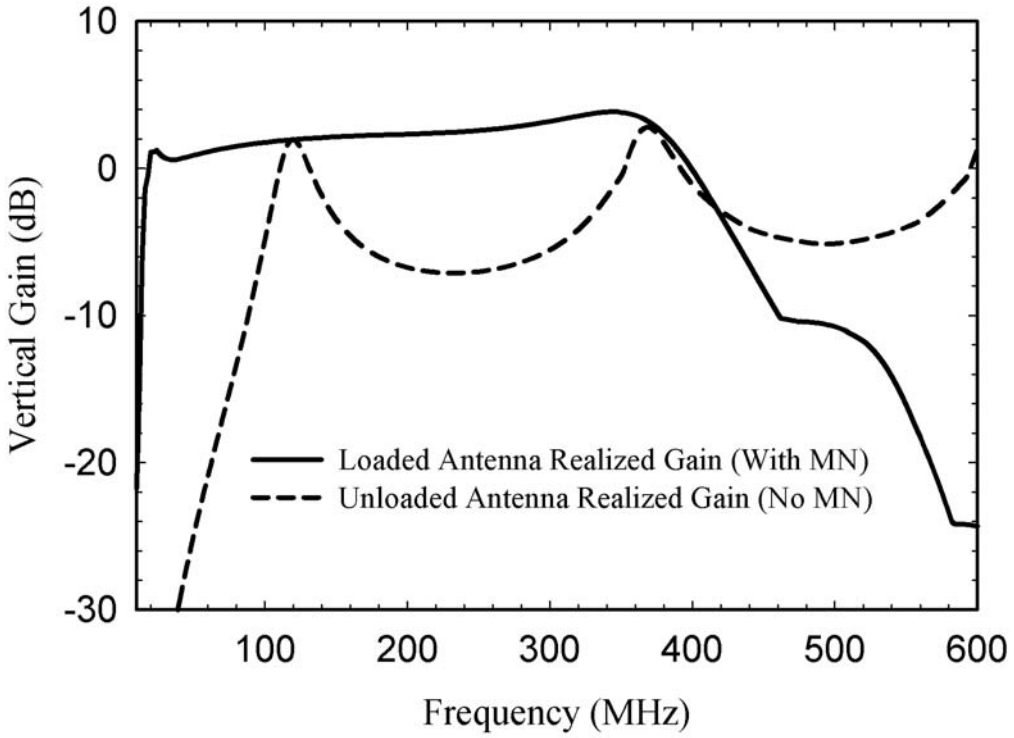

Figure 64 Approximately loaded dipole realized gain ($\theta = 90^{\circ}$) with matching network (MN) compared to the unloaded dipole realized gain without MN. The realized gain includes impedance mismatch losses

6.3.6 Realized Gain Analysis

Figure 64 summarizes the improved bandwidth of the *approximate loading* case compared to the *unloaded* case by comparing their overall realized gains (includes impedance mismatch losses). The *unloaded* case omits a passive matching network (seventh-order network designed using the RFT from 10-350 MHz) since it did not significantly improve the impedance bandwidth in that frequency range. This clearly demonstrates that the loading scheme leads to a more easily matched input impedance. The *approximate loading* case is clearly better than the *unloaded* case. The unloaded dipole manifests two different dipole modes below 400 MHz (see Figure 57), while the loaded antenna has only one (see Figure 60). The loaded antenna realized gain also varies far less over frequency compared to the unloaded dipole.

6.4 Conclusion

In this chapter, a design methodology was introduced to systematically design wideband, electrically small antennas, based on the theory of characteristic modes. This scheme can be used to implement an ideal desired antenna current distribution over a wide frequency range using a finite number of loads at a finite number of ports. The reactive loads at these ports are determined such that this current distribution resonates over a wide frequency band. As an example, the method was applied to a simple wire dipole antenna which was loaded with a set of reactive elements. For this antenna, it was found that non-Foster reactive elements were required to synthesize the reactances determined by equation(6.3). Furthermore, it has been demonstrated that through the

loading of a dipole antenna using non-Foster elements, the overall antenna bandwidth may be vastly improved. Both pattern and input impedance for the loaded dipole antenna were stabilized over a substantially wider frequency range compared to the unloaded dipole antenna, even without a matching network at the feed point. As expected, improved input impedance bandwidth was obtained when a passive matching network was introduced at the feed port.

CHAPTER 7

CONCLUSIONS

7.1 Summary and Conclusion

In this work a design procedure for designing wide band (both the input impedance bandwidth and the far field pattern bandwidth) electrically small to mid size antennas using the theory of Characteristic Modes (CM) and the theory of matching networks was presented. Another important goal of this work was the study of the behavior of the antenna input impedance as a function of the antenna's number of feeds and their locations.

A new model for antenna input impedance based of the theory of Characteristic Modes was presented. The development of this model was a key contribution to this dissertation as it contributes to the understanding of the resonance phenomena of the input impedance of antennas. This model was extensively used in the preceding chapters to design wideband small to mid size antennas. The model helped in showing that parallel resonance phenomena does not correspond to a single Characteristic Mode, but is rather due to an interaction of at least two nearby modes each having eigenvalues of opposite sign. This is in contrast to the series resonance phenomenon, which is mainly due to a single CM. A discussion of the rectangular microstrip patch antenna cavity modes and how these modes are related to CM were also discussed. It was concluded that the CM of the microstrip patch antenna do not correspond to its cavity modes.

A Vee shaped vertically polarized antenna was designed such that mainly one dominant mode is excited in the desired frequency band. High order modes can be suppressed in the desired frequency band by a proper design of the feeding network. Two feeds were used to excite the proper mode of the Vee shaped antenna to obtain vertical polarization; the right locations of the two feeds were chosen based on the knowledge of the antenna's CM.

Furthermore, a design technique applicable to both reconfigurable and wide band antennas that is based on the application of reactive loading was also presented. Passive loads were used in the design of a reconfigurable dipole antenna while non-foster reactive loads were used in the design of wide band dipole antenna; the load values were calculated such that they resonate the antenna with one dominant current mode at different single frequency points (reconfigurable antenna) or over the whole frequency band (wide band antenna). The technique is applicable to small to mid size antennas where high order current modes are not strongly excited.

7.2Future Work

- Apply the theory of CM to control the parallel resonance frequency point(s) of patch antennas mostly by loading it or by geometry modifications.
- Fabricate pattern reconfigurable antenna based on the theory of CM
- Fabricate and build antenna using NIC (Negative Impedance Converters) to use them as loads for designing wide band electrically small antennas.
- Apply more than two feeds for the antenna conformal to Manta UAV to extend the antenna bandwidth.

APPENDIX A

ELECTRICALLY SMALL ANTENNAS: QUALITY FACTOR

As it is well known, the smaller the value of the antenna quality factor Q the wider the antenna bandwidth. According to Chu [1], the Q factor of an antenna increases by decreasing its electrical size. Chu derived the minimum Q factor of an antenna that can be enclosed within a sphere of radius a. The derivation is for an Omni-directional antenna of arbitrary shape. The Q is derived as function of $ka=2\pi a/\lambda$ where a is the radius of a hypothetical sphere surface enclosing the antenna.

For a vertically polarized antenna Figure 65 the index of the first radiating spherical mode is TM_{01} which indicates that the antenna input impedance will be highly capacitive with low radiation resistance. The field outside the sphere can be expressed in terms of a complete set of TM_{0n} orthogonal waves propagating away from the sphere (where n is the index of each mode). Consequently Chu [1] replaced the space outside the sphere by a finite number (N) of independent equivalent circuits (Figure 66) where each has its independent characteristic impedance such that all the equivalent circuits are connected to the inside of the sphere with N number of ports with one port pulled outside the sphere to represent the input port.

The equivalent representation of each equivalent circuit Z_n (Figure 67) can be expressed as a cascade of series capacitance and shunt inductance terminated with a unit resistance (high pass filter). For n = 1 the equivalent circuit (see Figure 68) consists of

series capacitance and shunt inductance terminated with one Ω resistor. The unit resistor represents the radiation resistance of an infinitesimal dipole. The capacitance and inductance are proportional to the ratio a /c where c is the speed of light.

It can be shown that the minimum Q that can be obtained theoretically for n = 1, 2 & 3 in terms of ka ($2\pi a/\lambda$) [13] as follows:

$$
\begin{aligned}
Q_1 &= \frac{1}{k_0 a} + \frac{1}{\left(k_0 a\right)^3} \\
Q_2 &= \frac{3}{k_0 a} + \frac{6}{\left(k_0 a\right)^3} + \frac{18}{\left(k_0 a\right)^5} \\
Q_3 &= \frac{6}{k_0 a} + \frac{21}{\left(k_0 a\right)^3} + \frac{135}{\left(k_0 a\right)^5} + \frac{675}{\left(k_0 a\right)^7}
\end{aligned}
\tag{8.1}
$$

Figure 69 shows the minimum Q for n=1,2 and 3. For a small dipole antenna (n = 1) when ka is less than 1 the Q is very large and the input impedance is capacitive with very small real part. From a circuit point of view, since the series capacitance impedance in Figure 68 is proportional to 1/ka and the shunt inductance impedance is proportional to ka, when ka < 1 most of the generator voltage will appear as a voltage drop across the capacitor with very small voltage drop across the resistor which represents the antenna radiation "loss". In other words, most of the TM_{01} wave will be stored in the near field of an antenna that can be enclosed within a sphere of radius ka<1. The Same resultant applies to TM_{02} when ka < 2 and for TM_{03} when ka < 3.

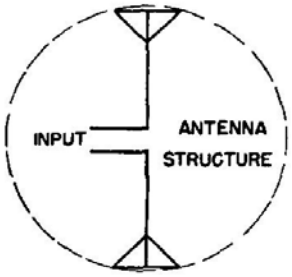

Figure 65 Schematic diagram of a vertically polarized Omni-directional antenna.

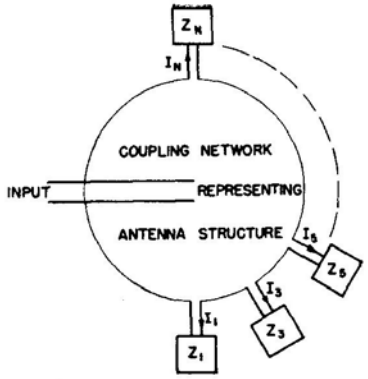

Figure 66 Equivalent circuit model of a vertically polarized Omni-directional antenna.

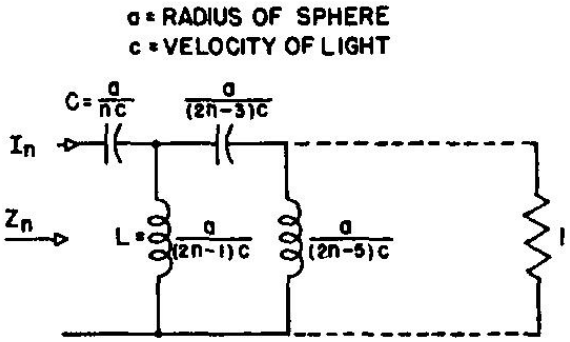

Figure 67 Equivalent Circuit of TM_{0n} Mode

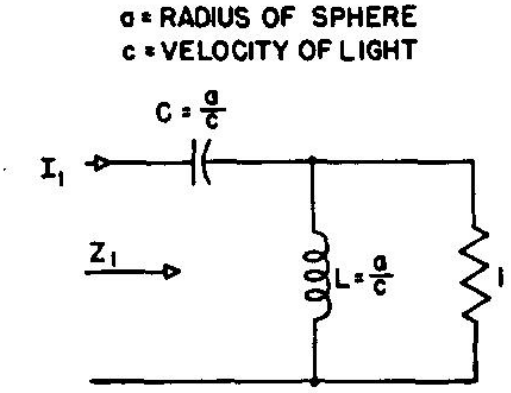

Figure 68 Equivalent Circuit of TM_{01} Mode (Electric Dipole)

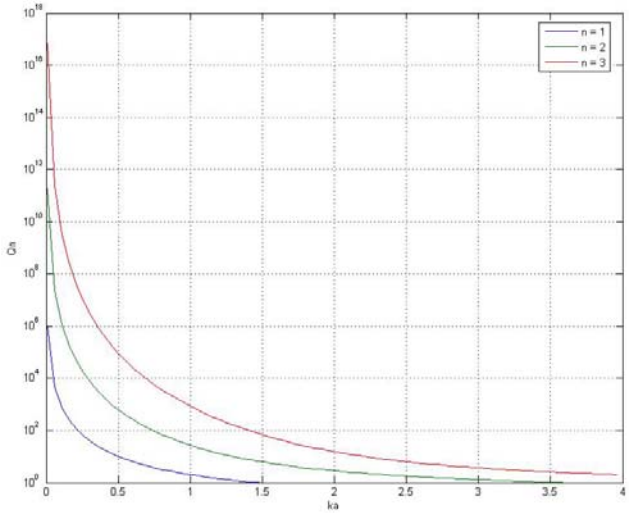

Figure 69 Q factor of the first three dominant modes of a dipole antenna.

The above analysis does not take into account any matching networks that can be incorporated into the antenna. It simply states that it is difficult to radiate energy with an antenna that is enclosed within a sphere that is electrically small. Although no specific antenna is mentioned, it is known that the Q will be lowered if the antenna occupies most of the volume of the sphere. That is why "thin" antennas have higher Q's than "fat" antennas. Thus, "fat" antennas are needed to increase the input impedance bandwidth.

As the design of the antenna proceeds, the input impedance and qualify factor of the antenna should be calculated to guide and help in determining whether the design is proceeding in the right direction. There are various expressions for the Q factor that have been used in the past. The definition used in this work is due to Yajian and Best [17] who define Q as follows:

$$Q(\omega) = \frac{\omega}{2R(\omega)} | Z_o^{'}(\omega) | \tag{8.2}$$

where $Z_o^{'}(\omega)$ is the derivative of $Z_o(\omega)$ with respect to the angular frequency ω. The "tuned" input impedance at the antenna terminals, $Z_o(\omega)$, is defined as

$$Z_o(\omega) = Z(\omega) + jX_s(\omega) = R(\omega) + j(X(\omega) + X_s(\omega)) \tag{8.3}$$

where $R(\omega)$ and $X(\omega)$ are the real and imaginary parts of the input impedance $Z(\omega)$, respectively, and $X_s(\omega)$ is the reactance added to the input impedance to "tune" the antenna such that the imaginary part goes to zero at the frequency ω. The derivative with respect to the frequency ω is given by

$$Z_o^{'}(\omega) = R'(\omega) + j\left(X'(\omega) + |X(\omega)|/\omega\right) \tag{8.4}$$

The expression in (8.4) is then used in (8.2) to evaluate the qualify factor of the antenna.

To take into account a matching network, Wideband matching network concepts developed in other fields (circuit theory) can be incorporated to antenna design to determine the maximum bandwidth that can be achieved. Algorithms, also developed in other fields, can be used to actually design the matching networks that are assumed to be lossless. Keeping in mind that all real components have some loss, the lossless assumption serves as an upper limit.

APPENDIX B

ELECTRICALLY SMALL ANTENNAS: MATCHING NETWORKS DESGIN USING REAL FREQUENCY TECHNIQUE (RFT) BANDWIDTH (MATCHING NETWORK INCLUDED)

The design and performance of the matching network is highly dependent on the frequency behavior of the input impedance of the antenna which becomes the load to the matching network. It is well known from Bode and Fano's work [16] that the wideband matching of a frequency dependent load is easier if the qualify factor (Q) of the load is as small as possible. This statement, known as the Bode-Fano criterion, can be written in mathematical form as follows:

$$\int_0^\infty \ln\left|\frac{1}{\Gamma(\omega)}\right| d\omega \le \frac{\pi\omega_o}{Q} \tag{9.1}$$

where Q is the quality factor of the load and $\Gamma(\omega)$ is the reflection coefficient looking into the lossless matching network. For example, if the maximum allowed value of $\Gamma(\omega)$ is set to Γ_m and the frequency bandwidth is $\Delta\omega$, (9.1) then reduces to

$$\Delta\omega \ln\left|\frac{1}{\Gamma_m}\right| \le \frac{\pi\omega_o}{Q} \tag{9.2}$$

It is clear from (9.2) that a smaller Q results in larger bandwidth. The impedance bandwidth of an antenna for a given VSWR level throughout the frequency band of

interest can be expressed assuming a series or parallel *RLC* representation of the antenna's input impedance as follows [19]:

$$BW = \frac{1}{Q}\sqrt{\frac{(TS-1)(S-T)}{S}} \quad where\left(BW = \frac{f_2 - f_1}{f_o}\right) \tag{9.3}$$

where Q is the quality factor, VSWR (f_1) = VSWR (f_2) = S (f_1 and f_2 are the lower and upper band edge frequencies around the resonant frequency f_o) and

$$T = \frac{Zo}{\mathrm{Re}(Z_{in}(f_o))} \tag{9.4}$$

where Z_o is the characteristic impedance of the transmission line connected to the antenna and Zin is the input impedance of the antenna at f_o. If the real part of the input impedance Zin(f_o) equals the characteristic impedance of the T-line, then T is equal 1 and the formula for BW reduces to the well know expression:

$$BW = \frac{1}{Q}\frac{S-1}{\sqrt{S}} \tag{9.5}$$

However; for maximum bandwidth, T ≠ 1. It can be shown that the optimum values of T is $T_{opt} = \frac{1}{2}\left(S + \frac{1}{S}\right)$. Thus, assuming we use the Q_1 for a small antenna (see equation (8.1)), the optimum bandwidth reduces to [15]:

$$BW = \frac{(ka)^3}{1+(ka)^2}\frac{S^2-1}{2S} \tag{9.6}$$

The above equation will be use to plot BW for various values of S.

Let us now consider the antenna and a matching circuit as depicted in Figure 70. Several theoretical methods [5] and [6] have been developed to determine an ideal matching network for wideband matching applications. In Figure 70, the matching network "sees" the frequency dependent input impedance of the antenna (calculated or measured) to the right and the generator or transmission line impedance Z_g to the left. Presented here are results based on the method developed by Carlin [7].

To establish the limits for small antennas, let us consider a small electrical dipole that radiates the TM_{01} mode. In other words, the antenna is replaced by the equivalent circuit shown in Figure 68. Following Carlin's method [7], the impedance bandwidth can be increased by using a matching circuit. This method not only provides the maximum theoretical bandwidth that can be achieved, but it also provides an algorithm to design the matching network. The formula below [15] gives the maximum fractional bandwidth BW_r assuming the load has a circuit representation in Figure 68 for Zin

$$BW_r = \frac{f_2 - f_1}{f_1} = n-1, \quad n \geq 1. \qquad BW_r = n-1 = \frac{1}{Y\,(W-ka)+1} - 1 \tag{9.7}$$

$$W = \sqrt[3]{-q+\sqrt{D}} - \sqrt[3]{q+\sqrt{D}} - \frac{Y\,(1-YKa)}{1+Y^2} \tag{9.8}$$

$$q = \frac{\left(2+3Y^{2}\left(Y^{2}+1\right)\right)(ka)^{3} - 3Y\left(Y^{2}-1\right)(ka)^{2}}{2\left(1+Y^{2}\right)^{3}} + \frac{3\left(Y^{2}-1\right)(ka) - Y\left(3+Y^{2}\right)}{2\left(1+Y^{2}\right)^{3}} \qquad (9.9)$$

$$p = \left(\frac{Yka-1}{1+Y^{2}}\right)^{2}$$

$$D = p^{3} + q^{2} > 0$$

The parameter $Y = \frac{-\pi}{\ln \rho_{\max}}$ and f_1 and f_2 are the lower and upper band edge frequencies where the magnitude of the reflection coefficient is less than $\rho_{\max}$

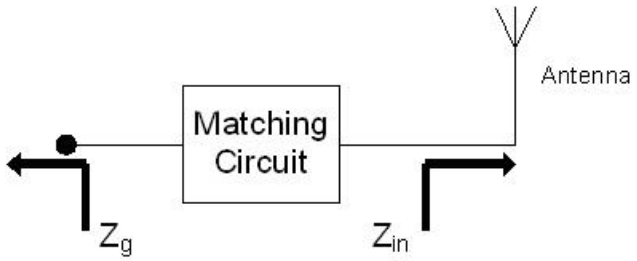

Figure 70 Antenna and matching circuit

The maximum impedance bandwidth the antenna with a matching circuit can reach is plotted in Figure 71 using equation(9.7). The curve for VSWR = 5 shows that we can obtain a relatively large impedance bandwidth at ka = 0.38 for VSWR ≥ 5. However for VSWR = 3 the ratio of f2/f1 is equal 1.4. On the other hand the curve for VSWR = 1.25 shows that the small electrical-dipole's fractional –bandwidth for VSWR ≤ 1.25 is very large for values of ka ≥ 0.7.

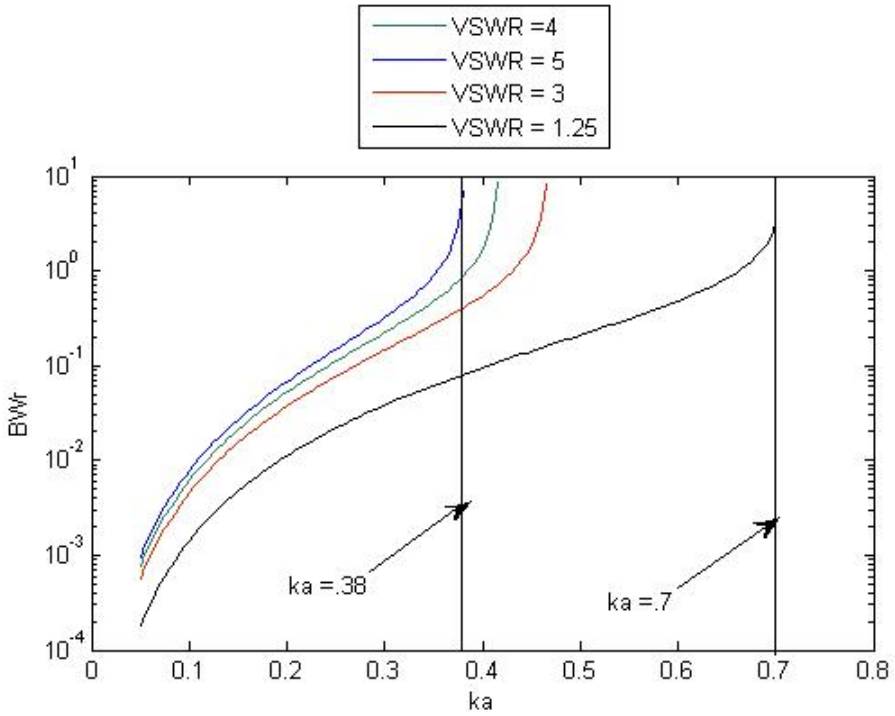

Figure 71 Upper limit for impedance bandwidth for different VSWR.

APPENDIX C

ELECTRICALLY SMALL ANTENNAS: MATCHING NETWORKS DESGIN USING REAL FREQUENCY TECHNIQUE (RFT)

Prior to the discussion of non-foster matching network design in which only negative inductors and negative capacitors are used a discussion of the real frequency technique [7] will be presented first. Figure 72 shows a cascade of the matching network (equalizer) under design and a unity terminated Darlington representation of a load. For maximum power transfer the unity normalized reflection coefficient S_2 is needed to be minimized by designing the equalizer with proper lossless elements. The input impedance looking at the input of the Darlington block toward the generator can be written a shown in (10.1)

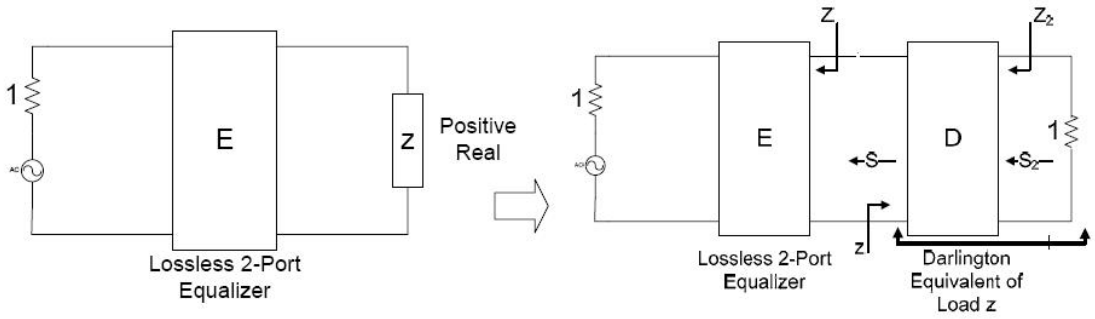

Figure 72 Blok diagram of cascade of Matching Network (Equalizer) and the Darlington representation of a load.

$$Z_2 = \frac{DZ + B}{CZ + A} \tag{10.1}$$

where A, B, C and D are the elements of the ABCD matrix of the equalizer and Z is the

input impedance looking from the output of the unity terminated equalizer (Figure 72)

$$S_2 = \frac{\frac{DZ+B}{CZ+A}-1}{\frac{DZ+B}{CZ+A}+1} \tag{10.2}$$

S_2 is the unit normalized reflectance measured at the input of the Darlington. After algebraic simplification [25] and using the fact that the circuit comprising the cascade of E and D is lossless S_2 can be written as in (10.3)

$$S_2 = b\,\frac{Z-z^*}{Z+z} \tag{10.3}$$

where z* is the load conjugate and b is the allpass Blaschke product which is formed on the RHP pole factors in z* [25]

It is easy to notice that the above formula for S_2 equals to the complex normalized reflectance S which is written in terms of z and Z.

To obtain maximum power transfer from the generator to the real part of the load the transducer power gain T(ω2) need to be maximized (minimize S_2):

$$T(\omega^2) = 1-\left|S_2(j\omega)\right|^2 = 1-\left|S(j\omega)\right|^2 \tag{10.4}$$

$$T(\omega^2) = \frac{4Rr}{\left|Z+z\right|^2},\ where\ r = \mathrm{Re}al\{z\}\ and\ R = \mathrm{Re}al\{Z\} \tag{10.5}$$

The rational positive real (PR) input impedance function Z of the equalizer is generated directly by an approximation procedure; Line-Segment of the real part R =Real(Z) (Figure 73) carried out at real frequency (Note no need to specify a transfer function). The imaginary part X of Z can be derived from its real part using Hilbert transform [25]:

$$R(\omega) = -\frac{1}{\pi}\int_{-\infty}^{\infty}\frac{X(\Omega)}{\Omega-\omega}d\Omega = -\frac{2}{\pi}\int_{0}^{\infty}\frac{\Omega X(\Omega)}{\Omega^2-\omega^2}d\Omega$$
$$X(\omega) = \frac{1}{\pi}\int_{-\infty}^{\infty}\frac{R(\Omega)}{\Omega-\omega}d\Omega = \frac{2\omega}{\pi}\int_{0}^{\infty}\frac{R(\Omega)}{\Omega^2-\omega^2}d\Omega \quad (10.6)$$

The real part of the measured load data z, r = Real (z), can also be approximated by piecewise line segment and the imaginary part of the load is deduced from the real part by Hilbert Transform (Note there is no need to specify circuit mode or analytical model for the load). The goal is to optimize the Transducer power gain by changing the slope of the piecewise segments of R to get the minimum lease square error or unconstrained multidimensional optimization. Once the optimum Z(ω) has been determined, the next step is its realization via lossless positive LC-network using Darlington.

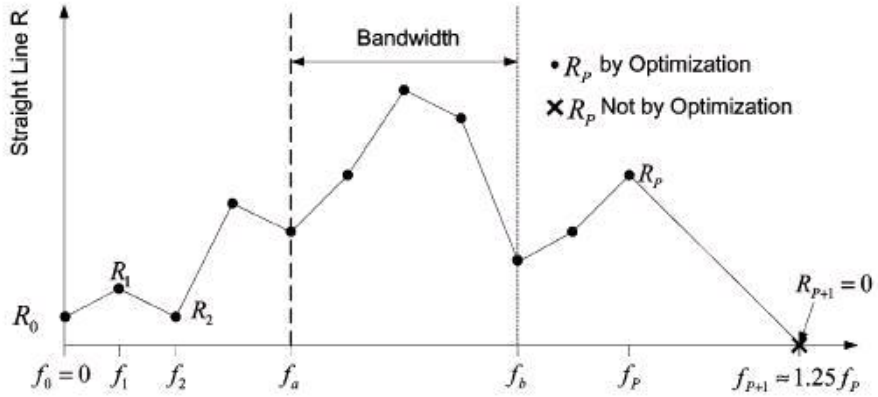

Figure 73 Pricewise representation of a resistive load

APPENDIX D

ELECTRICALLY SMALL ANTENNAS: MATCHING NETWORK WITH NON-FOSTER LOADS

The Real Frequency Technique provides a robust procedure to design passive matching network numerically. The theory on which the RFT is based can be extended to analytically designs ultra wideband matching network using non-foster loads.

Theoretically it is possible to obtain an infinite bandwidth with zero dB transducer gain, see equation (10.3), if Z as in Figure 74 is synthesized to equal to z* (conjugate of the load) at all frequency points. The lossless part of the Darlington representation of the positive real load z can be realized using only losels positive Inductors and Capacitors. However, the conjugate of the load z (z*) is realized only with negative inductors and capacitors. Figure 75 shows a matching network utilized using non-foster loads implemented by replacing each positive inductor (capacitor) of the Darlington representation of the load with inductor (capacitor) with the same magnitude but negative sign and connected back-to-back with the load. Negative Impedance Converters (NIC) [20], [21] and [22] can be used to utilize such components with the expense of increasing power consumption, complexity (i.e. stability) and noise floor.

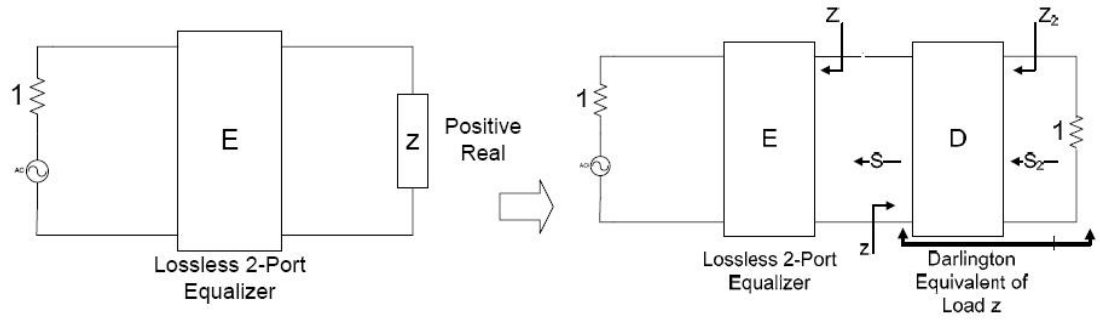

Figure 74 Blok diagram of cascade of Matching Network (Equalizer) and the Darlington representation of a load.

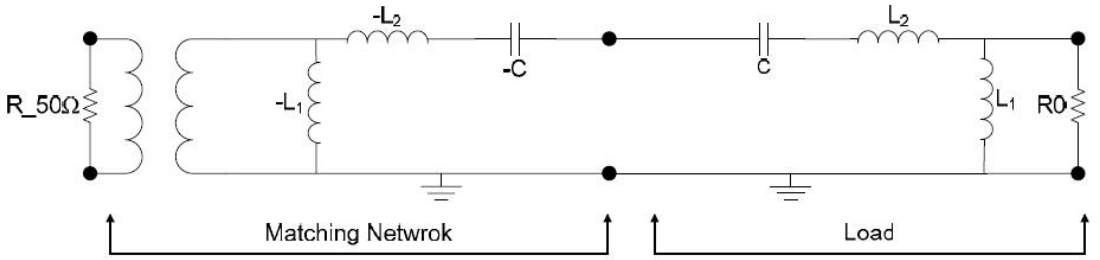

Figure 75 Matching network utilized using non-foster loads in cascade with positive real load

LIST OF REFERENCES

[1] L. Chu, “Physical limitations of omni-directional antennas,” J. Appl. Phys., vol. 19, pp. 1163–1175, 1948.
[2] H.A. Wheeler, “Fundamental Limits of Small Antennas,” Proceedings of The I.R.E. (IEEE), December 1947, pg. 1479-1484
[3] P. E. Mayes, “Frequency-independent antennas and broad-band derivatives thereof,” IEEE Proceedings, vol. 80, pp. 103–112, Jan. 1992.
[4] S. Licul, J. A. N. Noronha, W. A. Davis, D. G. Sweeney, C. R. Anderson, and T. M. Bielawa, “A parametric study of time-domain characteristics of possible uwb antenna architectures,” Vehicular Technology Conference, 2003. VTC 2003-Fall. 2003 IEEE 58th, vol. 5, pp. 3110–3114, 2003.
[5] S. Licul and W. A. Davis, “Pole/residue modeling of uwb antenna systems,” Antennas and ropagation Society International Symposium, 2004. IEEE, vol. 2, pp. 1748–1751, 2004.
[6] ——, “Unified frequency and time-domain antenna modeling and characterization,” Antennas and Propagation, IEEE Transactions on, vol. 53, no. 9, pp. 2882–2888, 2005.
[7] H.J. Carlin, “A new approach to gain-bandwidth problems,” IEEE Trans. Circuits and Systems, vol. CAS-24, April 1977
[8] R. Garbacz and R. Turpin, “A generalized expansion for radiated and scattered fields,” IEEE Trans. Antennas Propagat., vol. AP-19, no. 3, May 1971.
[9] R. Harrington and J. Mautz, “Theory of characteristic modes for conducting bodies,” IEEE Trans. Antennas Propagat., vol. AP-19, no. 5, pp. 622–628, Sept. 1971.
[10] ——, “Computation of characteristic modes for conducting bodies,” IEEE Trans. Antennas Propagat., vol. AP-19, no. 5, pp. 629–639, Sept. 1971.
[11] ——, “Pattern synthesis for loaded n-port scatterers,” IEEE Trans. Antennas Propagat., vol. AP-22, no. 2, pp. 184–190, Mar. 1974.
[12] ——, “Control of radar scattering by reactive loading,” IEEE Trans. Antennas Propagat., vol. AP-20, no. 4, pp. 446–454, Jul. 1972
[13] R. E. Collin and S. Rothschild, “Evaluation of antenna Q,” IEEE Trans. Antennas Propag., vol. 12, no. 1, pp. 23–27, Jan. 1964.
[14] H. F. Pues and A. R. Van de Capelle, “An impedance-matching technique for increasing the bandwidth of microtrip antennas,” IEEE Trans. Antennas Propag., vol. 37, no. 11, pp. 1345–1353, Nov. 1989.
[15] Arto Hujanen, Jan Holmberg, and Johan Carl-Erik Sten “Bandwidth Limitations of Impedance Matched Ideal Dipoles ” IEEE Transactions On Antennas And Propagation, Vol. 53, No. 10, October 2005
[16] R.M. Fano, “Theoretical limitations on the broadband matching of arbitrary impedances,” J. Franklin Inst., 1950, vol. 249, Aug 2002

[17] Arthur D. Yaghjian, and Steven R. Best," Impedance, Bandwidth, and Q of Antennas," IEEE TRANSACTIONS ON ANTENNAS AND PROPAGATION, VOL. 53, NO. 4, APRIL 2005
[18] www. agilent.com
[19] H. F. Pues and A. R. Van de Capelle, "An impedance-matching technique for increasing the bandwidth of microtrip antennas," IEEE Trans. Antennas Propag., vol. 37, no. 11, pp. 1345–1353, Nov. 1989.
[20] S. Sussman-Fort, "Gyrator-based biquad filters and negative impedance converters for microwaves," Int. J. Microwave Millimeter-Wave CAE, vol. 8, no. 2, pp. 86–101, 1998. [18] R. L.-R. James T.
[21] Aberle, Active Antennas With Non-Foster Matching Networks, ser. Synthesis Lectures on Antennas, C. A. Balanis, Ed. Morgan and Claypool Publishers, 2007.
[22] H. Kim, "Design of negative impedance converters for vhf and uhf applications," Master's thesis, Arizona State University, 2006.
[23] S. R. Best, "The Radiation Properties of Electrically Small Folded Spherical Helix Antennas," IEEE Trans. Antenna Propagat., vol. 52, pp. 953–960, April 2004.
[24] E. Newman. The electromagnetic surface patch code: Version 5, The Ohio State University. [Online]. Available: http://esl.eng.ohio-state.edu
[25] H. Carlin, P. Civalleri "Wideband Circuit Design"
[26] Weixia Wfu, Bin g-Zhong Wang, Xue-Song Yang, and Yong Zhang " A Pattern-Reconfigurable Planar Fractal Antenna and its Characteristic-Mode Analysis" IEEE Antennas and Propagation Magazine, Vol. 49, No. 3, June 2007
[27] P. E. Mayes, "Frequency-independent antennas and broad-band derivatives thereof," IEEE Proceedings, vol. 80, pp. 103–112, Jan. 1992.
[28] S. Licul, J. A. N. Noronha, W. A. Davis, D. G. Sweeney, C. R. Anderson, and T. M. Bielawa, "A parametric study of time-domain characteristics of possible uwb antenna architectures," Vehicular Technology Conference, 2003. VTC 2003-Fall. 2003 IEEE 58th, vol. 5, pp. 3110–3114, 2003.
[29] J. Quirin, "A study of high-frequency solid-state negative-impedance converters for impedance loading of dipole antennas," Master's thesis, University of Illinois, 1970.
[30] A. Poggio and P. Mayes, "Bandwidth extension for dipole antennas by conjugate reactance loading," IEEE Trans. Antennas Propagat., pp. 544– 547, Jul. 1971.
[31] R. C. Hansen, "Dipole arrays with non-foster circuits," Phased ArraySystems and Technology, 2003. IEEE International Symposium on, pp. 40–44, 2003.
[32] E. Antonino-Daviu, M. Cabedo-Fabr´es, M. Ferrando-Bataller, and A. Valero-Nogueira, "Wideband double-fed planar monopole antennas," Electronics Letters, vol. 39, pp. 1635–1636, 2003.
[33] M. Cabedo-Fabr´es, A. Valero-Nogueira, E. Antonino-Daviu, and M. Ferrando-Bataller, "Modal Analysis of a radiating Slotted PCB for Mobile Handsets," in The European Conference on Antennas and Propagation: EuCAP 2006, ser. ESA Special Publication, vol. 626, Oct. 2006.
[34] Khaled Obeidat, Bryan D. Raines, and Roberto G. Rojas "Frequency Reconfigurable Antenna Design Using The theory of Characteristic Modes" (Accepted to IEEE Trans. Antennas & Propagation April 2010)

[35] Khaled Obeidat, Bryan D. Raines, and Roberto G. Rojas "Application of Characteristic Modes and Non-Foster Multiport Loading to the Design of Broadband Antennas" Volume 58, Issue 1, January 2010
[36] R. Harrington and J. Mautz, "Modal analysis of loaded n-port scatterers,"IEEE Trans. Antennas Propagat., vol. AP-21, no. 2, pp. 188–199, Mar. 1973.
[37] Khaled Obeidat , Bryan D. Raines, and Roberto G. Rojas "Antenna Design and Analysis Using Characteristic Modes" 2007 IEEE AP-S International Symposium, Honolulu
[38] Khaled Obeidat , Bryan D. Raines, and Roberto G. Rojas "Design of Antenna Conformal to V-shaped Tail of UAV Based On the Method of Characteristic Modes " EWCA Berlin, Germany, March 23-27, 2009
[39] Khaled Obeidat , Bryan D. Raines, and Roberto G. Rojas "Design and Analysis of a Helical Spherical Antenna Using The Theory of Characteristic Modes" July, 2008, IEEE AP-S International Symposium, San Diego.
[40] Online: http://www.feko.info
[41] Cabedo-Fabres, M.; Antonio-Daviu, E.; Ferrando-Bataller, M.; Valero-Nogueira, A "On the use of characteristic modes to describe patch antenna performance" Antennas and Propagation Society International Symposium, 2003. IEEE, Volume 2, 22-27 June 2003, pp. 712–715 vol.2.
[42] Cabedo-Fabres, M.; Antonino-Daviu, E.; Valero-Nogueira, A.; Bataller, M.F. "The Theory of Characteristic Modes Revisited: A Contribution to the Design of Antennas for Modern Applications" Antennas and Propagation Magazine, IEEE, Volume 49, Issue 5, Oct. 2007, pp 52–68.
[43] S. D. Targonski and D. M. Pozar, "Design of wide-band circularly polarized aperture coupled microstrip antennas," IEEE Trans. Antennas Propagat., vol. 41, pp. 214-220, Feb. 1993.
[44] N. Behdad and K. Sarabandi., "A varactor-tuned dual-band slot antenna," Antennas and Propagation, IEEE Transactions on, vol. 54, no. 2, pp. 2882–2888, 2006.
[45] ——, "Dual-band reconfigurable antenna with a very wide tenability range," Antennas and Propagation, IEEE Transactions on, vol. 54, no. 2, pp. 2882–2888, 2006.
[46] L. S. and S. A., "Reconfigurable pifa antenna with ultrawideband tuning," in EuCAP, 2007, pp. 1–6.
[47] D. H. W. C. S. DeLuccia, M. F. P. P. L. Werner, and A. R. Bretones, "A novel frequency agile beam scanning reconfigurable antenna," in Antennas and Propagation Society International Symposium, 2004, pp. 1839– 1842.
[48] Agilent. Momentum. [Online]. Available: http://www.agilent.com
[49] Newman, E. H. "Small Antenna Location Synthesis Using Characteristic Modes", IEEE Transactions on Antennas and Propagation," AP-27, July 1979.
[50] Austin, B. A. and K. P. Murray, "The Application of Characteristic-Mode Techniques to Vehicle-Mounted NVIS Antennas," IEEE Transactions on Antennas and Propagation, AP-40, February 1998.